Tests of quantum chromodynamics in two-photon collisions and high-p_T photon production

William R. Frazer
University of California, San Diego, La Jolla, California 92093

John F. Gunion
University of California, Davis, California 95616

(Received 18 January 1979)

We use the diagrammatic approach to scale breaking to rederive the results of the renormalization-group approach to two-photon, $\gamma^*\gamma$, collisions, where one of the photons is highly virtual and the other nearly real. In an axial gauge only ladder diagrams contribute to leading-logarithmic accuracy. When interpreted in terms of the quark distribution of the real photon we obtain the result $G_{q/\gamma}(q^2,x) = [\alpha/\alpha_s(q^2)]\tilde{f}_q(x) + O(1)$, where $\tilde{f}_q(x)$ is an exactly calculable scaling function. By virtue of the fact that only ladder diagrams contribute in leading-logarithmic accuracy for this and other short-distance photon-target probes, we find that this form for $G_{q/\gamma}$ can be employed (to leading-logarithmic accuracy) in any short-distance application involving a photon target. We give a summary of these additional applications with emphasis on high-transverse-momentum phenomena. We present also estimates of the vector-dominance background to the pointlike component of the photon distribution function. In addition we present a convenient summary of leading-logarithmic quantum-chromodynamic corrections including dominant $x \to 1$ behaviors.

I. INTRODUCTION

Measurement of the two-photon process $\gamma^* + \gamma^* \to$ hadrons is possible in colliding lepton beams (Fig. 1). Interest in this process, first aroused by Brodsky, Kinoshita, and Terazawa,[1] has been heightened by the realization that it provides clean tests of quantum chromodynamics (QCD). Consider first the total cross section, proportional to the imaginary part of the forward amplitude $\gamma^*(q) + \gamma^*(p) \to \gamma^*(q) + \gamma^*(p)$, as in Fig. 2. The "doubly-deep" inelastic limit

$$|q^2| \to \infty, \quad |p^2| \to \infty \qquad (1.1)$$
$$\omega = \frac{2p\cdot q}{|q^2|} \sim \text{constant}, \quad \frac{p^2}{q^2} \sim \text{constant}$$

is the easiest to analyze. This analysis was first carried out by Gross and Treiman[2] using light-cone commutators, but is much simpler in renormalization-group language. The result is that in the limit (1.1), in the Euclidean region or continued to the physical region with the usual smoothing of threshold singularities, the amplitude is dominated by those terms of lowest order in the strong coupling constant $\alpha_s(q^2)$, the quark-loop diagrams in Fig. 3.

Although the Gross-Treiman limit (1.1) is most convenient for theoretical analysis, it is most inconvenient for measurement. Letting one of the photons $\gamma(p)$ be nearly real, consider the region of deep-inelastic scattering from a nearly real photon, $\gamma^*(q) + \gamma(p) \to$ hadrons,

$$|q^2| \to \infty, \quad p^2 \simeq 0, \quad \omega = \frac{2p\cdot q}{|q^2|} \text{ fixed}. \qquad (1.2)$$

Using the equivalent-photon approximation one can analyze the cross section in terms of photon structure functions $W_{1\gamma}$ and $W_{2\gamma}$, or $W_{1\gamma}$ and $W_{L\gamma}$, where

$$W_L \sim \tfrac{1}{2}\nu\omega W_2 - W_1, \qquad (1.3)$$

with $\nu = p\cdot q$. The contributions, to leading order in $\log q^2$, of the box diagram of Fig. 3 to these structure functions are[3,4]:

$$(W_{1\gamma})_{\text{box}} = e^4 \frac{3}{8\pi^2} \sum_{i=1}^{n_f} Q_i^4 [x^2 + (1-x)^2] \ln\left(\frac{|q^2|}{m_i^2}\frac{1-x}{x}\right) + O(1) \qquad (1.4a)$$

$$(W_{L\gamma})_{\text{box}} = e^4 \frac{3}{2\pi^2} \sum_{i=1}^{n_f} Q_i^4 x(1-x). \qquad (1.4b)$$

(We have extracted the color factor explicitly; our sums are only over quark flavor, e.g., $n_f = 4$ in the u, d, s, c model.) The fact that the leading term in $(W_{1\gamma})_{\text{box}}$ violates scaling, behaving like $\ln q^2$, whereas $(W_{L\gamma})_{\text{box}}$ violates the Callan-Gross relation, was pointed out by Walsh and Zerwas[5] and by Kingsley.[6] These terms originate from the fact that the photon, unlike hadrons, can produce partons of large

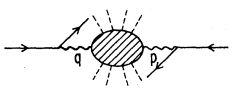

FIG. 1. A two-photon collision.

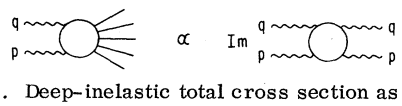

FIG. 2. Deep-inelastic total cross section as the imaginary part of $\gamma^*(q)\gamma \to \gamma\gamma^*(q)$.

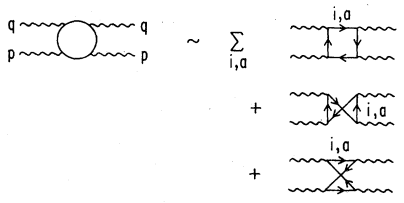

FIG. 3. The simplest "bare-box" contributions to $\gamma^*\gamma \to \gamma\gamma^*$.

transverse momentum by means of the "hard" process of direct production of a quark-antiquark pair.

Turning from the parton model to quantum chromodynamics (QCD), the box diagram remains an important contribution to the structure functions.[7] It is not, however, dominant. As we shall see, all ladder diagrams such as the one shown in Fig. 4(a) contribute to the leading behavior of $W_{1\gamma}$, whereas $W_{L\gamma}$ receives contributions also from ladders with the top rung crossed, as in Fig. 4(b). The important conclusion remains valid, that the leading contributions to $W_{1\gamma}$ and $W_{L\gamma}$ are *completely calculable* in QCD. That is, the leading term in $W_{1\gamma}$ is proportional to $\ln q^2$ with calculable coefficient, whereas the leading term in $W_{L\gamma}$ is a calculable function of the Bjorken scaling variable. Thus the two-photon process achieves a fundamental status in QCD, comparable to that of the e^+e^- annihilation cross section, in that the leading behavior of the structure functions is completely determined—not just the evolution in Q^2, as in the case of hadron structure function.

These conclusions were already obtained by Witten[8] by a renormalization-group operator-product analysis. The main contribution of the present work is the application of a diagrammatic method described in a previous paper.[9] In addition to providing confirmation of an important result, this method allows one to gain insight into the diagrams of which the result is composed. As for a hadron target, the leading-logarithmic contributions to $W_{1\gamma}$ arise entirely from ladder diagrams (with a mixture of quark and gluon rungs) when an axial gauge is employed. As usual, we may interpret

$$W_{1\gamma} = 3 \sum_{q,\bar{q}\ \text{flavors}} W_{1\gamma}^{i}$$

in terms of the per-color distribution function for a quark of type i in a real photon[3]; we obtain, per color,

$$G_{q_i/\gamma}(x, q^2) = \frac{2W_{1\gamma}^{i}}{Q_i^2} = \frac{\alpha}{\alpha_s(q^2)}\, \tilde{f}_i(x)\,, \tag{1.5}$$

where $\tilde{f}_i(x)$ is a scaling function calculated in the next section. Because the ladder structure of the QCD contributions is preserved (in the leading-logarithmic order) when a photon target is probed by any other short-distance process, this distribution function is universally applicable. Thus, for instance,[10] if we consider $\gamma_1 \to q_1\bar{q}_1$, $\gamma_2 \to q_2\bar{q}_2$ followed by $q_1q_2 \to q_1'q_2'$ via gluon exchange at high momentum transfer, Fig. 5, the cross section for q_1' at high p_T will exhibit exact scaling,

$$E_1' \frac{d\sigma}{d^3p_1'}(\gamma_1\gamma_2 \to q_1') \underset{90^\circ\text{c.m.}}{=} \frac{1}{(p_T)^4} f\left(x_T = \frac{2p_T}{\sqrt{s}}\right) + O\left(\frac{1}{\ln q^2}\right); \tag{1.6}$$

the $1/\alpha_s(q^2)$ behaviors in q_1/γ_1 and q_2/γ_2 are cancelled by the behavior of the cross section

$$(d\sigma/dt)(q_1q_2 \to q_1'q_2') \propto |\alpha_s(q^2)|^2$$

(here $|q^2| \sim 4p_T^2$). Two-photon collisions increase markedly the number of cross sections for which exact QCD predictions can be made; the complications which are typical of reactions involving hadrons are not present in the leading-logarithmic order.

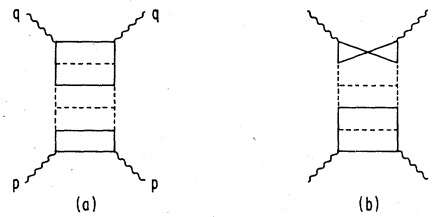

FIG. 4. Typical higher-order contributions to (a) $W_{1\gamma}$ and (b) $W_{L\gamma}$, from the $\gamma^*\gamma \to \gamma\gamma^*$ amplitude. Solid lines indicate quarks, dotted lines gluons, and wavy lines photons.

II. CALCULATION OF THE PHOTON STRUCTURE FUNCTIONS: MOMENT APPROACH

Having already calculated in the previous paper[9] (hereafter referred to as I) the leading amplitudes for $q\bar{q} \to \gamma^*\gamma^*$, we can calculate $\gamma\gamma \to \gamma^*\gamma^*$ simply by attaching two additional photons as shown in Fig. 6. Since the two-particle irreducible (2PI) photon-attachment amplitudes C_F and C_G have the leading behavior shown in Fig. 7, we need only calculate

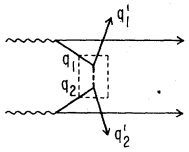

FIG. 5. A typical high-p_T jet production mechanism in $\gamma\gamma$ collisions; the short-distance subprocess $qq \to qq$ (in the box) is illustrated.

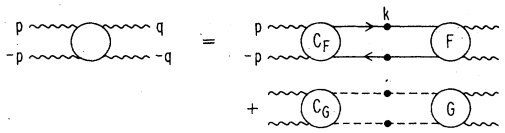

FIG. 6. Representation of the $\gamma\gamma \to \gamma^*\gamma^*$ amplitude in terms of a Bethe-Salpeter equation involving $gg \to \gamma^*\gamma^*$ and $qq \to \gamma^*\gamma^*$, and the kernels $\gamma\gamma \to gg$ and $\gamma\gamma \to qq$. Solid circles on intermediate lines and vertices indicate full, renormalized propagators and vertices.

the diagram shown in Fig. 8. We use the expansion for the $q\bar{q} \to \gamma^*\gamma^*$ amplitude given in I(3.7a) [this notation refers to Eq. (3.7a) of the previous paper] to obtain the result, averaged over spins of the target photon $\gamma(p)$,

$$T_{1\gamma} = e^4 3 \times (-2) \times \frac{4\nu}{q^2} \sum_{n=0}^{\infty} \int \frac{d^4k}{(2\pi)^4} \frac{(\ln k^2)^{\bar{\gamma}_F}}{k^2(k-p)^2} \left(\frac{2q\cdot k}{q^2}\right)^{n-1} \times [C_S f^S_{1,n}(k^2, q^2) + C_{NS} f^{NS}_{1,n}(k^2, q^2)] . \tag{2.1}$$

Here the factor of 3 is from summing over colors, the factor of -2 from closing a fermion loop and summing over quark and antiquark contributions (see Ref. 3) and 4ν comes from the traces (where we have momentarily included only the Feynman-gauge portion, $\sum \epsilon_\alpha \epsilon^*_\beta = -g_{\alpha\beta}$, of the target-photon polarization sum). The $f_{1,n}$'s include both the crossed and uncrossed virtual-photon contributions. The $(\ln k^2)^{+\bar{\gamma}_F}$ arises from the combination of $C_F(p,k)(\ln k^2)^{-\bar{\gamma}_F}$ behaving as $(\ln k^2)^{\bar{\gamma}_F}$. An expression for $\bar{\gamma}_F$ is given later.

The singlet and nonsinglet notation of (2.1) is slightly different from I; assuming that only $Q = \frac{2}{3}$ and $Q = -\frac{1}{3}$ quarks occur it is useful to define

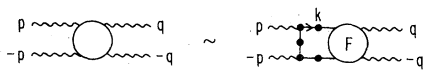

FIG. 8. The simplified leading-logarithmic calculation of $\gamma\gamma \to \gamma^*\gamma^*$ based on the kernel behaviors of Fig. 7 which show that only the $\gamma\gamma \to qq$ kernel survives in leading-logarithmic order.

$$f^S_{\alpha,n} \equiv \sum_{i=1}^{n_f} f^i_{\alpha,n} ,$$
$$f^{NS}_{\alpha,n} \equiv f^{12}_{\alpha,n} = f^1_{\alpha,n} - f^2_{\alpha,n} , \tag{2.2}$$

where the flavor indices refer to $u=1, d=2, s=3$, $c=4, \ldots$. The coefficients C_S and C_{NS} are defined as follows:

$$\sum_{i=1}^{n_f} Q_i^2 f^i_{\alpha,n} = C_S f^S_{\alpha,n} + C_{NS} f^{NS}_{\alpha,n} , \tag{2.3}$$

where

$$C_S = \frac{4n_u + n_d}{9n_f} = \frac{1}{n_f} \sum_{i=1}^{n_f} Q_i^2 ,$$
$$C_{NS} = \frac{1}{3} \frac{n_u n_d}{n_f} = (Q_1^2 - Q_2^2) \frac{n_u n_d}{n_f} , \tag{2.4}$$

with n_u the number of quarks of charge $\frac{2}{3}$ and n_d the number of quarks of charge $-\frac{1}{3}$. For the four-flavor model $n_f = 4$,

$$C_S = \tfrac{5}{18} , \quad C_{NS} = \tfrac{1}{3} . \tag{2.5}$$

We perform the integration in (2.1) using the angular integration identity quoted in I(B7) and the asymptotic forms for $f^S_{1,n}$ and $f^{NS}_{1,n}$ quoted in I(C.3a) and I(3.11). For the leading term (see Sec. IV for a discussion of nonleading terms) we obtain[11]

$$T_{1\gamma} = e^4 \ln(Q^2/\Lambda^2) \sum_{n=1}^{\infty} 3 \times 2\omega^n \left[\frac{C_{NS} F_1^{NS}}{1 + \gamma^n_{FF}/2b} + C_S \left(\frac{C^{1,n}_{11}}{1+\gamma^n_1} + \frac{C^{1,n}_{12}}{1+\gamma^n_2} \right) \right] , \tag{2.6a}$$

where $Q^2 = |q^2|$; or, using the identities of Appendix IC and the expression for F_1^{NS} in I(3.9c) (repeated in Appendix A),

$$T_{1\gamma} = e^4 \ln(Q^2/\Lambda^2) \sum_{n=1}^{\infty} 12\bar{\gamma}_n \omega^n \left[\frac{C_{NS}/3}{1 + \gamma^n_{FF}/2b} + \frac{n_f C_S^2}{d_n} (1 + \gamma^n_{VV}/2b) \right] . \tag{2.6b}$$

Following Witten's notation[8] we have defined

$$d_n \equiv 1 + (\gamma^n_{VV} + \gamma^n_{FF})/2b + (\gamma^n_{VV}\gamma^n_{FF} - \gamma^n_{FV}\gamma^n_{VF})/4b^2 \tag{2.7a}$$

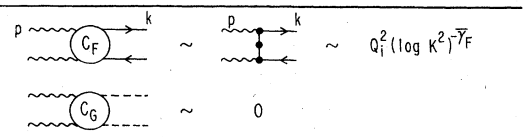

FIG. 7. The leading-logarithmic behavior of the kernels.

where b is defined by reference to the moving coupling constant

$$\bar{g}^2(q^2) \sim \frac{1}{b \ln(Q^2/\Lambda^2)} ,$$
$$16\pi^2 b \equiv \bar{b} = [\tfrac{11}{3} C_2(G) - \tfrac{4}{3} n_f T(R)] = (11 - \tfrac{2}{3} n_f) \tag{2.7b}$$

in the case $C_2(G) = 3$, $C_2(R) = \frac{4}{3}$, $T(R) = \frac{1}{2}$ appropriate to QCD.

In the calculation outlined, one would find $\bar{\gamma}_n^{-1} = 8\pi^2 n$. There is, however, a further complication

which we have been ignoring: The contribution of nonladder graphs in which an external virtual photon line is crossed with a real photon line. In the Feynman gauge of the external real photon, which we used in deriving Eq. (2.1), such crossed diagrams do contribute in leading order. One finds, however, by using the same reasoning as we used in I, Sec. III A, that one can avoid having these crossed diagrams contribute to leading order by putting the target photon (with momentum p) in Lipatov gauge,[12] where $q\cdot\epsilon = 0$. The correct version of Eq. (2.1) is then found by a calculation of the ladder graphs formally identical to that given in Appendix B of I, up to I(B10), to yield Eq. (2.6), but with

$$\bar{\gamma}_n = \frac{1}{8\pi^2}\,\frac{n^2+n+2}{n(n+1)(n+2)}\,. \tag{2.8}$$

In order to apply these results in the physical region we consider the moments of $W_1 = \mathrm{Im}T_1/2\pi$, with the result[13]

$$\begin{aligned} W_{1\gamma,n} &\equiv \int_0^1 W_{1\gamma}(x,q^2)\,x^{n-1}dx \\ &= e^4 3\bar{\gamma}_n \ln\!\left(\frac{Q^2}{\Lambda^2}\right)\left[\frac{n_f C_S^{\,2}(1+\gamma^n_{VV}/2b)}{d_n} + \frac{C_{NS}}{3}\,(1+\gamma^n_{FF}/2b)^{-1}\right]. \end{aligned} \tag{2.9}$$

Thus the moments are exactly calculable in terms of the anomalous dimensions γ^n_{VV}, etc., which appear directly and in d_n. The QCD expressions for the γ's are given in Appendix A.

It is useful to rewrite (2.9) in the final general form

$$W_{1\gamma,n} = e^4 \ln\!\left(\frac{Q^2}{\Lambda^2}\right)\left[\frac{\left(\sum_{i=1}^{n_f} Q_i^{\,2}\right)^2}{n_f}\,3\bar{f}_{S,n} + \frac{\left(n_f\sum_{i=1}^{n_f} Q_i^{\,4} - \left(\sum_{i=1}^{n_f} Q_i^{\,2}\right)^2\right)}{n_f}\,3\bar{f}_{NS,n}\right] \tag{2.10a}$$

where

$$\bar{f}_{S,n} \equiv \frac{1+\gamma^n_{VV}/2b}{d_n}\,\bar{\gamma}_n,\quad \bar{f}_{NS,n} \equiv \frac{\bar{\gamma}_n}{1+\gamma^n_{FF}/2b} \tag{2.10b}$$

It is interesting to compare Eq. (2.10) with the result of calculating the simple quark-loop diagram, uncorrected by gluon exchange:

$$(W_{1\gamma,n})_{\mathrm{box}} = e^4 3\bar{\gamma}_n \sum_{i=1}^{n_f} Q_i^{\,4}\ln(Q^2/m_i^{\,2})\,, \tag{2.11}$$

where m_i and Q_i are the masses and charges of the quarks. The net effect of the ladder corrections, as shown in Fig. 4(a), has been to modify the numerical value of the coefficient of the leading behavior, which is proportional to $\ln Q^2$, but not to change the power of $\ln Q^2$ (the quark mass is also replaced by the scale parameter Λ). Of course, (2.10) reduces to (2.11) if the γ_{FF}, γ_{FV}, etc., $\to 0$. The reason the power persists unmodified, in contrast to the behavior of a hadronic structure function, can be traced to the hard-photon vertices in Fig. 7. The logarithmic factor associated with C_F is $(\ln k^2)^{-\bar{\gamma}_F}$, as we discussed in I(2.20). If the photons were replaced by gluons, for example, the appropriate power would be $(\ln k^2)^{-1-\bar{\gamma}_F-\bar{\gamma}_G}$. Most significant is the softening of the vertex by the factor $\alpha_s(k^2)\sim(\ln k^2)^{-1}$. By contrast, the photon vertices yield simply e^2, which we take to be constant.

The calculation of $W_{L\gamma}$ proceeds similarly; making use of the expression I(3.19) for the $p_\mu p_\nu W_{\mu\nu} = \frac{1}{2}\nu\omega W_L$ projection, we obtain

$$\tfrac{1}{2}\nu\omega T_{L\gamma} = \tfrac{1}{2}\nu\omega(T_{L\gamma})_{\mathrm{box}} + e^4 3\times 2\times 4\nu\,\frac{\nu^2}{q^4}\sum_{n=0}^{\infty}\int\frac{d^4k}{(2\pi)^4}\left(\frac{2q\cdot k}{q^2}\right)^{n-1}\frac{(\ln k^2)^{\bar{\gamma}_F}}{k^2(k-p)^2}\,\left[C_S\,f^S_{L,n}(k^2,q^2) + C_{NS}\,f^{NS}_{L,n}(k^2,q^2)\right] \tag{2.12}$$

for the $(-g_{\alpha\beta})$ part of the target-photon polarization sum; including the other pieces of the polarization sum in the Lipatov gauge and performing the integrations yields

$$T_{L\gamma} = (T_{L\gamma})_{\mathrm{box}} + e^4\ln\!\left(\frac{Q^2}{\Lambda^2}\right)\sum_{n=1}^{\infty} 6\bar{\gamma}_n\omega^n\left[\frac{C_{NS}F^{NS}_{L,n}}{1+\gamma^n_{FF}/2b} + C_S\left(\frac{C^{L,n}_{11}}{1+\gamma_1} + \frac{C^{L,n}_{12}}{1+\gamma_2}\right)\right], \tag{2.13}$$

and, using I(C12),

$$T_{L\gamma} = (T_{L\gamma})_{\mathrm{box}} + e^4\ln\!\left(\frac{Q^2}{\Lambda^2}\right)\sum_{n=1}^{\infty} 6\bar{\gamma}_n\omega^n\left\{\frac{C_{NS}F^{NS}_{L,n}}{1+\gamma^n_{FF}/2b} + \frac{C_S}{d_n}\left[F^S_{L,n}(1+\gamma^n_{VV}/2b) + G^S_{L,n}\gamma^n_{FV}/2b\right]\right\}. \tag{2.14}$$

Expressions for $F^{NS}_{L,n}$, $F^S_{L,n}$, and $G^S_{L,n}$ (the "Born" terms in the ladder development of T_L) were obtained in I(3.20) and are repeated in Appendix A; they include both crossed and uncrossed virtual-photon diagrams. The F_L's arise entirely from the graphs with one gluon loop. This means we need to add the contribution of the bare-no-gluon box diagram which has the same scaling behavior as (2.14). The absence of the bare box diagram in the $F_{L,n}$'s is evident from comparison of Fig. 7 and Fig. I13(b). We have left out

the box diagram in (2.14) and must add it in separately. Alternatively, one could return to Eq. I(3.19) and add another amplitude to recapture the box diagram.

Making use of the expressions for the F_L's and G_L's we obtain finally

$$T_{L\gamma} = (T_{L\gamma})_{\text{box}} + e^4 \sum_{n=1}^{\infty} \frac{6\bar{\gamma}_n \omega^n}{2\pi^2 b(n+1)} \left[\frac{1}{3} \frac{C_2(R) C_{\text{NS}}}{1+\gamma^n_{FF}/2b} + \frac{n_f C_S^{\,2}}{d_n} \left(C_2(R)(1+\gamma^n_{VV}/2b) + \frac{4T(R)}{n+2} \frac{\gamma^n_{FV}}{2b} \right) \right] . \tag{2.15}$$

Again, to apply this result in the physical region one takes moments of $W_L = 1/2\pi \operatorname{Im} T_L$,

$$W_{L\gamma,n}(q^2) \equiv \int_0^1 W_{L\gamma}(x, q^2) x^{n-1} dx . \tag{2.16}$$

For the box diagram one finds [see (1.4b)]

$$[W_{L\gamma,n}(q^2)]_{\text{box}} = e^4 3 \sum_{i=1}^{n_f} Q_i^{\,4} \frac{1}{2\pi^2} \frac{1}{(n+1)(n+2)} . \tag{2.17}$$

For the rest we use $\frac{1}{4}$ the coefficient of ω^n in Eq. (2.15) (see Ref. 13). One can express the result in the form

$$\frac{W_{L\gamma,n}}{(W_{L\gamma,n})_{\text{box}}} \sim 1 + \frac{n^2+n+2}{n(n+1)16\pi^2 b} \left[\frac{C_{\text{NS}}}{3\sum_{i=1}^{n_f} Q_i^{\,4}} \frac{C_2(R)}{1+\gamma^n_{FF}/2b} + \frac{n_f C_S^{\,2}}{d_n \sum_{i=1}^{n_f} Q_i^{\,4}} \left(C_2(R)(1+\gamma^n_{VV}/2b) + \frac{4T(R)}{n+2} \frac{\gamma^n_{FV}}{2b} \right) \right] . \tag{2.18}$$

In the four-flavor model, where $\sum_{i=1}^{n_f} Q_i^{\,4} = \frac{34}{81}$, $C_{\text{NS}} = \frac{1}{3}$, and $n_f C_S^{\,2} = \frac{25}{81}$, the above expression agrees with Witten's Eq. (14).[8] Note, however, that Witten's b (call it b_W) is normalized such that $b_W = 8\pi^2 b$, where b has the conventional normalization given in (2.7b).

III. CALCULATION OF THE DISTRIBUTION FUNCTIONS, $G_{q/\gamma}(q^2,x)$ AND $G_{q/\gamma}(q^2,x)$.

In this section we rederive the results of Sec. II using the light-cone, probability function approach of Sec. IV of I. We consider only $W_{1\gamma}$, though similar techniques can be employed for $W_{L\gamma}$, and restrict ourselves to the nonsinglet part of the structure function. We begin with the diagrams of Fig. 6, with the current attachment kernels having the asymptotic behavior of Fig. 7.

The $q\bar{q} \to \gamma^*\gamma^*$, quark-color-average T_1 amplitude was given asymptotically in I(4.2) as

$$A(k,q) \sim b(q^2, k^2, k\cdot q) \not{q} . \tag{3.1}$$

The structure function W_1^i, for a quark of flavor i, is related to b by[3,11]

$$W_1^i(q^2, p^2, x) = \frac{1}{2\pi} \operatorname{Im}[2p\cdot q\, b^i(q^2, p^2, p\cdot q)] . \tag{3.2}$$

The moments of W_1^i have the behavior, for the nonsinglet part [I(4.18)]

$$W^i_{1,n}(q^2, p^2) \sim \frac{e^2}{2} Q_i^{\,2} \left(\frac{\ln(|q^2|/\Lambda^2)}{\ln(|p^2|/\Lambda^2)} \right)^{-\gamma^n_{FF}/2b} \times \left[\ln\left(\frac{|p^2|}{\Lambda^2} \right) \right]^{-\bar{\gamma}_F} . \tag{3.3}$$

The $(\ln|p^2|)^{-\bar{\gamma}_F}$ factor is present until we renormalize the external quark line carrying p. The expressions for $\gamma^n_{FF}/2b$ and $\bar{\gamma}_F$ appear in Appendix A.

We then calculate the photon amplitude T_1, Fig. 8, coming from attaching the target photon to a quark of given color and of flavor i as

$$e^2(-Q_i^{\,2}) \int \frac{d^4k}{(2\pi)^4} \frac{(\ln k^2)^{\bar{\gamma}_F}}{k^4(p-k)^2} \times \operatorname{Tr}[\gamma_\mu \not{k} b^i(q^2, k^2, k\cdot q) \not{q} \not{k} \gamma_\nu (\not{p} - \not{k})] \times P^\gamma_{\mu\nu}(p) , \tag{3.4}$$

where

$$P^\gamma_{\mu\nu}(p) = \frac{1}{2} \left(-g_{\mu\nu} + \frac{p_\mu q_\nu + p_\nu q_\mu}{p\cdot q} - \frac{q^2}{\nu^2} p_\mu p_\nu \right)$$

is the spin-average Lipatov-gauge polarization sum. This gauge, as discussed in Sec. II, eliminates nonladder graphs. As in I Sec. IV we write $d^4k = dk^2 d^2k_\perp dz/2z$, where

$$k = \left(zP + \frac{k^2 + k_\perp^{\,2}}{4zP}, k_\perp, zP - \frac{k^2 + k_\perp^{\,2}}{4zP} \right) \tag{3.5}$$

in a light-cone frame. We evaluate the dk^2 integral by picking up the $[1/(p-k)]^2$ pole, giving $k^2 \sim -k_\perp^{\,2}/(1-z)$, take $(1/2\pi)\operatorname{Im}$, and obtain for the contribution to the photon target's $W_{1\gamma}$ from a quark or antiquark of given color and of flavor i

$$W^i_{1\gamma}(q^2, p^2, x) = \frac{e^2 Q_i^{\,2}}{8\pi^2} \int^{Q^2} \frac{dk_\perp^{\,2}}{k_\perp^{\,2}} (\ln k_\perp^{\,2})^{\bar{\gamma}_F} \times \int_x^1 \frac{dz}{z} [z^2 + (1-z)^2] \times W_1^i(q^2, k^2, x/z) , \tag{3.6}$$

where $k^2 = -k_\perp^{\,2}/(1-z)$

W_1^i incorporates all QCD corrections to the bare

quark i structure function coming from ladders with quark-line-i sides and gluon rungs. Note from (3.3) that its moments reduce to the bare result $W^i_{1,n} = \frac{1}{2} Q_i^2 e^2$ when $\gamma^n_{FF} \to 0$. Recalling[3] that the per color contribution to W_1 of a quark of given flavor i can be interpreted as the per color distribution function of that quark in the given target T by

$$W^i_{1T}(x) = \frac{e^2}{2} Q_i^2 G_{q_i/T}(x) \tag{3.7}$$

we see that (3.6) is equivalent to

$$G_{q_i/\gamma}(q^2, p^2, x) = \int_x^1 \frac{dz}{z} G^{\text{bare}}_{q_i/\gamma}(z, k_\perp^2) d^2k_\perp \times G^{\text{QCD}}_{q_i/q_i}(q^2, k^2, x/z), \tag{3.8}$$

where, for large $k_\perp^2$,

$$G^{\text{bare}}_{q_i/\gamma}(z, k_\perp^2) \sim \frac{e^2 Q_i^2}{8\pi^3} \frac{1}{k_\perp^2} [z^2 + (1-z)^2] \tag{3.9}$$

is the pointlike distribution of a single quark of given color in the photon as calculated from the direct plus crossed bare-box photon diagrams. As an aside, note that we can derive (1.4a) as (including antiquarks)

$$[W_{1\gamma}(x)]_{\text{box}} = e^2 3 \times 2 \sum_{i=1}^{n_f} \frac{Q_i^2}{2} \int^{Q^2} \pi dk_\perp^2 G^{\text{bare}}_{q_i/\gamma}(x, k_\perp^2). \tag{3.10}$$

In Eq. (3.8)

$$G^{\text{QCD}}_{q_i/q_i}\left(q^2, k^2, \frac{x}{z}\right) \equiv \frac{2}{e^2 Q_i^2} (\ln k^2)^{\bar\gamma_F} W_1^i(q^2, k^2, x/z)$$

is the fully renormalized distribution for a final quark of fixed color summed over initial quark colors, including all leading-logarithmic QCD corrections. Eq. (3.8) shows that the full probability distribution function for a quark in a photon is obtained by the natural convolution of the bare-quark-in-a-photon distribution function with this QCD-corrected quark-in-a-quark distribution.

Taking moments of (3.6) and using (3.3) we obtain for a given color and flavor quark or antiquark

$$W^i_{1\gamma,n} = e^4 \frac{Q_i^4}{2} \frac{\bar\gamma_n \ln(Q^2/\Lambda^2)}{1 + \gamma^n_{FF}/2b} = e^4 \frac{Q_i^4}{2} \bar f_{\text{NS},n} \ln(Q^2/\Lambda^2), \tag{3.11a}$$

where

$$e^2 \bar\gamma_n = \frac{\alpha}{2\pi} \frac{n^2+n+2}{n(n+1)(n+2)} \tag{3.11b}$$

is the z^{n-1} moment of $k_\perp^2 G^{\text{bare}}_{q_i/\gamma}$ of (3.9).

If γ_{FV} or γ_{VF} is set equal to zero, corresponding to retaining only the fermion-sided ladder graphs with gluon rungs, one finds from (2.10b) that

$$\bar f_{S,n} = \bar f_{\text{NS},n} \tag{3.12}$$

and we see that after summation of (3.11) over quarks and antiquarks of all flavors and colors we obtain exactly the result (2.10) for this special case. The form (3.11) is actually a good approximation to the more complete expression obtained with γ_{FV} and γ_{VF} retained as given in Appendix A. Using (3.7) to convert to a per-color distribution function, we can restate (3.11) as

$$\int_0^1 G_{q_i/\gamma}(q^2, x) x^{n-1} dx = e^2 Q_i^2 \ln(Q^2/\Lambda^2) \bar f_{\text{NS},n}. \tag{3.13}$$

This is equivalent [using $\ln(Q^2/\Lambda^2) = 1/4\pi b \alpha_s(q^2)$)] to the statement that

$$G_{q_i/\gamma}(q^2, x) = Q_i^2 \frac{\alpha}{\alpha_s(q^2)} \frac{\bar f_{\text{NS}}(x)}{4\pi b}; \tag{3.14}$$

all the moments have the same scaling behavior in q^2 in the form of a universal multiplicative factor. More generally, including the singlet contributions by extracting the coefficients of Q_i^2 in (2.10), we obtain for a quark of given color

$$\int_0^1 G_{q_i/\gamma}(q^2, x) x^{n-1} dx = e^2 \ln \frac{Q^2}{\Lambda^2} \left(Q_i^2 \bar f_{\text{NS},n} + \frac{\sum_{j=1}^{n_f} Q_j^2}{n_f} (\bar f_{S,n} - \bar f_{\text{NS},n}) \right), \tag{3.15}$$

which is the result of the convolution (3.8) using the full $G^{\text{QCD}}_{q_i/q_j}(q^2, k^2, x/z)$ including singlet contributions. Namely, from I, Appendix C, the distribution *per color of q_i summed over q_j colors*, is

$$\int_0^1 G^{\text{QCD}}_{q_i/q_j}(q^2, k^2, \tau) \tau^{n-1} d\tau = \delta_{ij} [\xi(q^2, k^2)]^{-\gamma^n_{FF}/2b} + \frac{1}{2n_f} \{ [\xi(q^2, k^2)]^{-\gamma_1^n} D_{11}^n + [\xi(q^2, k^2)]^{-\gamma_2^n} D_{12} - [\xi(q^2, k^2)]^{-\gamma^n_{FF}/2b} \} \equiv \delta_{ij} h_D^n(\xi) + \frac{1}{2n_f} h_{ND}^n(\xi), \tag{3.16}$$

where

$$\xi(q^2,k^2)=\frac{\ln(|q^2|/\Lambda^2)}{\ln(|k^2|/\Lambda^2)}\,.$$

The $1/2n_f$ occurs because the number of quarks and antiquarks of all flavors is $2n_f$; δ_{ij} is diagonal in that i and j must have the same flavor including quark or antiquark nature. In the above

$$\begin{aligned}
D^n_{11}&=\frac{\gamma^n_{FF}/2b-\gamma^n_{VV}/2b-\delta^n}{-2\delta^n}\,,\\
D^n_{12}&=\frac{\gamma^n_{VV}/2b-\gamma^n_{FF}/2b-\delta^n}{-2\delta^n}\,,\\
\delta^n&=\frac{1}{2b}\left[(\gamma^n_{FF}-\gamma^n_{VV})^2+4\gamma^n_{FV}\gamma^n_{VF}\right]^{1/2},\\
\gamma^n_{1,2}&=\frac{1}{2}\left(\frac{\gamma^n_{FF}}{2b}+\frac{\gamma^n_{VV}}{2b}\mp\delta^n\right).
\end{aligned}\tag{3.17}$$

By taking moments of the convolution of $G^{\text{bare}}_{q_j/\gamma}$ and $G^{\text{QCD}}_{q_i/q_j}$ we obtain an integral equation involving the product of the moments

$$\begin{aligned}
&\int_0^1 G_{q_i/\gamma}(q^2,p^2,x)x^{n-1}dx\\
&\quad=e^2\sum_{j=1}^{2n_f}Q_j^{\,2}\int_{k^2=p^2}^{k^2=q^2}d\left(\ln\frac{|k^2|}{\Lambda^2}\right)\bar\gamma_n\\
&\qquad\times\int_0^1 d\tau\,\tau^{n-1}G^{\text{QCD}}_{q_i/q_j}(q^2,k^2,\tau)\,,
\end{aligned}\tag{3.18}$$

yielding (3.15) after using the identity

$$\frac{D^n_{11}}{1+\gamma^n_1}+\frac{D^n_{12}}{1+\gamma^n_2}=\frac{1+\gamma^n_{VV}/2b}{d_n}\,.\tag{3.19}$$

One should, of course, note that

$$W_{1\gamma}=e^2 3\times 2\sum_{i=1}^{n_f}Q_i^{\,2}\left[\tfrac{1}{2}G_{q_i/\gamma}(q^2,x)\right],\tag{3.20}$$

with $G_{q_i/\gamma}$ given by (3.15), is equivalent to our earlier result (2.10).

With these techniques it is now easy to obtain a second important result, the gluon distribution in a photon $G_{g/\gamma}$. We compute it using the convolution

$$\begin{aligned}
G_{g/\gamma}(q^2,p^2,x)=&\sum_{i=1}^{2n_f}\int_x^1\frac{dz}{z}\,d^2k_\perp G^{\text{bare}}_{q_i/\gamma}(z,k_\perp^{\,2})\\
&\times G^{\text{QCD}}_{g/q_i}(q^2,k^2,x/z)\,.
\end{aligned}\tag{3.21}$$

G^{QCD}_{g/q_i} is averaged over gluon colors but summed over quark colors. We require only the moments of G^{QCD}_{g/q_i}; these are easily obtained from I, where we computed the moments of $G^{\text{QCD}}_{q_i/g}$, by the reflection $\gamma_{VF}\leftrightarrow\gamma_{FV}$. We obtain, after summing over gluon colors as well as q_i colors [the net sum yielding a factor $(N^2-1)T(R)=NC_2(R)$, where N^2-1 is the number of gluons].

$$\begin{aligned}
&(N^2-1)\int_0^1 d\tau\,\tau^{n-1}G^{\text{QCD}}_{g/q_i}(q^2,k^2,\tau)\\
&\quad\equiv Nh^n_G(\xi)\\
&\quad=N[D^n_{21}\xi(q^2,k^2)^{-\gamma^n_1}+D^n_{22}\xi(q^2,k^2)^{-\gamma^n_2}]
\end{aligned}\tag{3.22}$$

with ξ of Eq. (3.16) and

$$D^n_{21}=-D^n_{22}=\frac{\gamma^n_{FV}}{2b}\,\frac{2}{\delta^n}\,.\tag{3.23}$$

The $C_2(R)$ factor, mentioned above, is absorbed into γ^n_{FV} and there is a minus sign coming from effectively closing a quark loop.

Performing the $d^2k_\perp$ integration from (3.21) (after taking moments as in (3.18)) we obtain

$$\begin{aligned}
&(N^2-1)\int_0^1 G_{g/\gamma}(q^2,x^2,\tau)\tau^{n-1}d\tau\\
&\quad=e^2 2N\sum_{i=1}^{n_f}Q_i^{\,2}\ln\left(\frac{Q^2}{\Lambda^2}\right)\bar\gamma_n\,\frac{\gamma^n_{FV}}{2b}\,\frac{2}{d_n}\,\frac{\gamma^n_2-\gamma^n_1}{\delta^n}\,.
\end{aligned}\tag{3.24}$$

For the color average we thus have (using $\gamma^n_2-\gamma^n_1=\delta^n$)

$$\begin{aligned}
&\int_0^1 G_{g/\gamma}(q^2,p^2)\tau^{n-1}d\tau\\
&\qquad=\frac{2N}{(N^2-1)}\,e^2\sum_{i=1}^{n_f}Q_i^{\,2}\ln\left(\frac{Q^2}{\Lambda^2}\right)\frac{\bar\gamma_n 2\gamma^n_{FV}}{2bd_n}\,,
\end{aligned}\tag{3.25}$$

with $N=3$ colors in the standard theory.

We can run a consistency check on the normalization of $G_{g/\gamma}$ by checking that momentum is conserved. The momentum $\int xGdx$ corresponds to $n=2$. Thus we should have the QCD-corrected momentum sum equal to the momentum sum predicted by the bare-box diagram, i.e.,

$$\begin{aligned}
&2N\sum_{i=1}^{n_f}\int G_{q_i/\gamma}(x)xdx+(N^2-1)\int G_{g/\gamma}(x)xdx\\
&\quad=2N\sum_{i=1}^{n_f}\int G^{\text{bare}}_{q_i/\gamma}(x)xdx\,.
\end{aligned}\tag{3.26}$$

Using (3.15) and (3.25) this becomes [factoring out the common piece, $2\sum_{i=1}^{n_f}e^2Q_i^{\,2}\bar\gamma_n\ln(Q^2/\Lambda^2)$]

$$N\left(\frac{1+\gamma^n_{VV}/2b}{d_n}+\frac{2\gamma^n_{FV}}{2bd_n}\right)_{n=2}=N\,.\tag{3.27}$$

For $n=2$, $\gamma^n_{VV}\gamma^n_{FF}-\gamma^n_{VF}\gamma^n_{FV}=0$ so that $d_n=1+\gamma^n_{VV}/2b+\gamma^n_{FF}/2b$; also, for $n=2$, $2\gamma^n_{FV}=\gamma^n_{FF}$ and we see that (3.27) is satisfied.

Note that, unlike the hadron-target case, the amount of momentum carried by the gluons, in leading-logarithmic order, is a fixed fraction of the total

$$\frac{\text{quark momentum}}{\text{gluon momentum}} = \frac{1+\gamma_{VV}^{n=2}/2b}{2\gamma_{FV}^{n=2}/2b} = \frac{(11/3)C_2(G)}{(8/3)C_2(R)} = \frac{99}{32}, \tag{3.28}$$

independent of Q^2 and n_f. Corrections to (3.28) are of order $[\ln\ln(Q^2/\Lambda^2)]/\ln(Q^2/\Lambda^2)$, whereas for a hadron target this ratio approaches its constant limit much more slowly as $Q^2\to\infty$. For $n=2$ we find that $\gamma_1^n=0$ and the γ_1^n term dominates as $Q^2\to\infty$ in (3.22) and (3.16) yielding

$$\begin{aligned}\frac{\text{quark momentum}}{\text{gluon momentum}} &= \frac{N\sum_{i=1}^{2n_f} G_{q_i/q_j}^{\mathrm{QCD}n=2}}{(N^2-1)G_{g/q_j}^{\mathrm{QCD}n=2}} = \frac{\gamma_{VV}^{n=2}}{2\gamma_{FV}^{n=2}} \\ &= \frac{1}{2}\frac{n_f T(R)}{C_2(R)} = \frac{1}{2}\frac{Nn_f}{(N^2-1)} \\ &= \frac{\frac{1}{2}\times(\text{No. of quarks})}{\text{No. of gluons}} = \frac{3}{4}\frac{n_f}{4}.\end{aligned} \tag{3.29}$$

Asymptotically much more momentum is carried by gluons in a hadron than in a photon if $n_f=4$. The value of n_f at which these fractions become equal is precisely $n_f=\frac{33}{2}$, the critical value at which assymptotic freedom is lost.

In summary, (3.15) and (3.25) are the crucial results for a quark and gluon distribution, after all QCD corrections, in a photon target. To actually obtain the distribution functions we must, of course, invert the moment results. We will pursue this in the next section, where we also estimate the background coming from the vector-meson dominated part of the photon.

IV. APPLICATIONS AND PHENOMENOLOGY

A. Nonleading terms in $W_{1\gamma}$

In the previous sections we have calculated the leading contributions, proportional to $\alpha_s^{-1}(Q^2) \sim \ln Q^2$, to the deep-inelastic scattering from a real or nearly real photon. In principle this is the simplest two-photon process, the total cross section for a highly virtual photon on a photon target, being totally inclusive and requiring no measurement of the hadronic final states.

Although in principle the leading term we have calculated in $W_{1\gamma}$—call it $W_{1\gamma}^{\mathrm{PL}}$ because it arises from the pointlike character of the photon—is measureable by extracting the coefficient of $\ln Q^2$ in $W_{1\gamma}$; in practice the measurement will be much easier in a region of x and Q^2 where the background is small compared to the leading term. In this section we estimate the magnitude of the "theoretical background," the non-leading contributions, in $W_{1\gamma}$.

Let us write the moments $W_{1\gamma,n}$ in a form which exhibits the dependence of the leading terms on $\alpha_s(Q^2)$:

$$W_{1\gamma,n}(Q^2) = W_{1\gamma,n}^{\mathrm{PL}}(Q^2) + W_{1\gamma,n}^{\mathrm{H}}(Q^2), \tag{4.1a}$$

where

$$W_{1\gamma,n}^{\mathrm{PL}}(Q^2) = \frac{\overline{W}_{1\gamma,n}^{\mathrm{PL}}}{\alpha_s(Q^2)}[1+O(\alpha_s)] \tag{4.1b}$$

and

$$W_{1\gamma,n}^{\mathrm{H}}(Q^2) = \sum_a A_n^a[\alpha_s(Q^2)]^{\lambda_{a,n}}[1+O(\alpha_s)], \tag{4.1c}$$

where the $\lambda_{a,n}$, the eigenvalues of the anomalous-dimension matrix, are positive definite (except for the case $n=2$, when one of them is zero). In this paper we have calculated $\overline{W}_{1\gamma,n}^{\mathrm{PL}}/\alpha_s(Q^2)$ and the result is given in Eq. (2.9). We have also calculated $W_{L\gamma,n}^{\mathrm{PL}}$, which has an expansion like (4.1c) but with all terms multiplied by a factor α_s. The higher-order corrections to $W_{1\gamma}^{\mathrm{PL}}$ in (4.1b) are also calculable in QCD by calculating multiloop diagrams.[14]

On the other hand, $W_{1\gamma,n}^{\mathrm{H}}$ is like a hadronic structure function in that its absolute magnitude is not calculable in QCD perturbation theory—its magnitude is not determined by short-distance phenomena. It arises from the low-k^2 portion of the region of integration in (2.1), which in turn depends on the unknown small-p^2 behavior of the function $A_n(p^2)$ in I (3.11). This is, of course, the analog of the unknown matrix elements of the operators in the operator-product expansion. It is important to understand what Q^2's are necessary before $W_{1\gamma}^{\mathrm{H}} \ll W_{1\gamma}^{\mathrm{PL}}$.

Although we cannot calculate $W_{1\gamma}^{\mathrm{H}}$ we can estimate it by assuming vector-meson dominance, $W_{1\gamma}^{\mathrm{H}} \approx W_{1\gamma}^{\mathrm{VMD}}$. A rather quick estimate of the VMD contribution can be obtained from the quark-counting form[15]

$$\begin{aligned} &xG_{q/\rho/\gamma}^{\text{bare VMD}}(x) = \tfrac{1}{3}\tfrac{1}{4}C_\rho(1-x)\frac{4\pi\alpha}{f_\rho^2}, \\ &\frac{f_\rho^2}{4\pi} = 2.2, \quad C_\rho = 1.0, \end{aligned} \tag{4.2}$$

for any $q=u$, $\bar{u}$, d, or $\bar{d}$ of any one color. We take $xG_{q/\rho}(x)=\frac{1}{12}C_\rho(1-x)$ corresponding to the simplest quark counting prediction for $x\to 1$; the value of C_ρ is chosen so that after summing over u, $\bar{u}$, d, and $\bar{d}$ of all colors, the quarks carry in combination 50% of the ρ's momentum. The resulting contribution to $W_{1\gamma}$ (from 3.20) is

$$\begin{aligned} W_{1\gamma}^{\mathrm{VMD}} &= 3e^2\sum_{\substack{u,\bar{u}\\ d,\bar{d}}} Q_i^{\,2}\,\tfrac{1}{2}\times\tfrac{1}{12}C_\rho\frac{(1-x)}{x}\frac{4\pi\alpha}{f_\rho^2} \\ &= 4.6\times10^{-4}\frac{1-x}{x}e^2, \end{aligned} \tag{4.3a}$$

so that

$$W_{1\gamma,n}^{\text{bare VMD}}=\frac{4.6\times10^{-4}e^2}{n(n-1)}. \tag{4.3b}$$

We compare this to the bare-box result

$$(W_{1\gamma,n}^{\text{PL}})_{\text{box}}=3\times2\times e^2\sum_{i=1}^{n_f}\frac{Q_i^2}{2}\frac{\alpha}{2\pi}\ln\left(\frac{Q^2}{m^2}\right)\frac{n^2+n+2}{n(n+1)(n+2)} \tag{4.4}$$

$$=1.5\times10^{-3}e^2\ln\left(\frac{Q^2}{m^2}\right)\frac{n^2+n+2}{n(n+1)(n+2)}.$$

The experiments will measure, on average, the momentum moment ($n=2$), which yields

$$\frac{W_{1\gamma,n=2}^{\text{VMD bare}}}{(W_{1\gamma,n=2}^{\text{PL}})_{\text{box}}}\sim\frac{0.5}{\ln(Q^2/m^2)}. \tag{4.5}$$

For $Q^2\gtrsim2$ GeV^2 and $m=0.5$ GeV this is less than 25%. In addition, the ratio of distribution functions can be made arbitrarily small by looking in the $x\to1$ region. For the naive forms discussed so far

$$\frac{W_{1\gamma}^{\text{bare VMD}}}{(W_{1\gamma}^{\text{PL}})_{\text{box}}}\underset{x\to1}{\propto}(1-x). \tag{4.6}$$

This relative enhancement of pointlike pieces as $x\to1$ is preserved after all QCD corrections are incorporated. To see this, we first must obtain an $x\to1$ expression for G_{q_i/q_j}^{QCD}.[16] The $x\to1$ limit is controlled by the large-n moments. As $n\to\infty$ γ_{FV} and $\gamma_{VF}\to0$ as $1/n$ relative to γ_{VV} and γ_{FF}. The final result is then controlled entirely by γ_{FF} ($\bar f_{\text{NS}}\to\bar f_{\text{S}}$ as $\gamma_{FV},\gamma_{VF}\to0$),

$$\frac{\gamma_{FF}^n}{2b}\underset{n\to\infty}{\sim}\frac{4}{\bar b}C_2(R)(\ln n+\gamma_E-\tfrac{3}{4}), \tag{4.7}$$

where $\bar b=16\pi^2b=11-\frac{2}{3}n_f$ and γ_E is Euler's constant. This leads to the result, from (3.3),

$$\int_0^1 G_{q_i/q_j}^{\text{QCD}}(q^2,k^2,x)x^{n-1}dx \underset{n\to\infty}{\sim}\delta_{ij}\left(\frac{\ln(|q^2|/\Lambda^2)}{\ln(|k^2|/\Lambda^2)}\right)^{-\gamma_{FF}^n/2b} \tag{4.8}$$

for the fully renormalized distribution defined below Eq. (3.10).

We look for a form

$$G_{q_i/q_i}^{\text{QCD}}(q^2,k^2,x)=N(1-x)^{p-1} \tag{4.9}$$

such that

$$\int_0^1 G_{q_i/q_i}^{\text{QCD}}x^{n-1}dx=\frac{N\Gamma(p)\Gamma(n)}{\Gamma(n+p)}=\left(\frac{\ln(|q^2|/\Lambda^2)}{\ln(|k^2|/\Lambda^2)}\right)^{-[4C_2(R)/\bar b](\ln n+\gamma_E-3/4)}. \tag{4.10}$$

The solution is[17,18]

$$N=\frac{e^{p(3/4-\gamma_E)}}{\Gamma(p)}, \tag{4.11a}$$

with

$$p=\frac{4C_2(R)}{\bar b}\ln\left(\frac{\ln(|q^2|/\Lambda^2)}{\ln(|k^2|/\Lambda^2)}\right). \tag{4.11b}$$

We may now convolute this form according to Eq. (3.8) to obtain[16,17]

$$G_{q_i/\gamma}^{\text{PL}}(q^2,p^2,x)\underset{x\to1}{\sim}e^2\int_{k^2\sim p^2}^{k^2\sim p^2}\frac{dz}{z}\frac{dk_\perp^2}{k_\perp^2}\frac{Q_i^2}{8\pi^2}[z^2+(1-z)^2]\frac{e^{p(3/4-\gamma_E)}}{\Gamma(p)}(1-x/z)^{p-1} \tag{4.12}$$

In the limit $x\to1$, the replacement $z=1-(1-x)\beta$ $(0<\beta<1)$ makes it clear that $z\to1$. In addition, we use

$$\frac{dk^2}{k^2}=-dp\frac{\bar b}{4C_2(R)}e^{-\left(p\frac{\bar b}{4C_2(R)}\right)}\ln\left(\frac{|q^2|}{\Lambda^2}\right) \tag{4.13}$$

to finally obtain after β integration

$$G_{q_i/\gamma}^{\text{PL}}(q^2,p^2,x)\underset{x\to1}{\sim}-e^2\ln\left(\frac{Q^2}{\Lambda^2}\right)\frac{Q_i^2}{8\pi^2}\frac{\bar b}{4C_2(R)} \tag{4.14}$$

$$\times\int_{(4C_2/\bar b)\ln[\ln(|q^2|/\Lambda^2)/\ln(|p^2|/\Lambda^2)]}^0 dp\frac{(1-x)^p\exp\{-p[\bar b/4C_2(R)+\gamma_E-3/4]\}}{p\Gamma(p)}.$$

The upper limit, $p=0$, dominates in leading logarithmic order and we have

$$[\lim_{p\to0}p\Gamma(p)=1]$$

$$G_{q_i/\gamma}^{\text{PL}}(q^2,p^2,x)\underset{x\to1}{\sim}e^2\frac{Q_i^2}{8\pi^2}\frac{\bar b}{4C_2(R)}\ln\left(\frac{Q^2}{\Lambda^2}\right)\left[\frac{\bar b}{4C_2(R)}+\gamma_E-\frac{3}{4}-\ln(1-x)\right]^{-1}, \tag{4.15}$$

which can be written in the form

$$G^{\mathrm{PL}}_{q_i/\gamma}(q^2,p^2,x)\underset{x\to 1}{\sim}\frac{{Q_i}^2\alpha}{2\pi\alpha_s(q^2)}\frac{4\pi}{\{\bar{b}-(3-4\gamma_E)C_2(R)+4C_2(R)\ln[1/(1-x)]\}}, \tag{4.16}$$

exhibiting a logarithmic suppression as $x\to 1$. For the vector-dominance piece, we compute (for $q=u,\ \bar{u},\ d,$ or $\bar{d}$)[19]

$$\begin{aligned}G^{\mathrm{VMD}}_{q/\rho/\gamma}(q^2,p^2,x)&=\int_x^1\frac{dz}{z}G^{\text{bare VMD}}_{q/\rho/\gamma}(z)G^{\mathrm{QCD}}_{q/q}(x/z)\\&\underset{x\to 1}{\sim}\int_x^1\frac{dz}{z}\tfrac{1}{12}C_\rho\frac{(1-z)}{z}\frac{4\pi\alpha}{f_\rho^2}\\&\quad\times\frac{e^{p(3/4-\gamma_E)}}{\Gamma(p)}\left(1-\frac{x}{z}\right)^{p-1},\end{aligned} \tag{4.17}$$

where the $\int dk^2$ has been incorporated into $G^{\text{bare VMD}}_{q/\rho/\gamma}$ and we have used the forms (4.2) and (4.9). Changing variables to $z=1-(1-x)\beta$ and performing the β integral as $x\to 1$, we obtain[20]

$$\begin{aligned}G^{\mathrm{VMD}}_{q/\rho/\gamma}(q^2,p^2,x)&\underset{x\to 1}{\sim}(1-x)^{p+1}\frac{C_\rho}{12}\frac{4\pi\alpha}{f_\rho^2}\\&\quad\times\frac{e^{p(3/4-\gamma_E)}}{\Gamma(p+2)}.\end{aligned} \tag{4.18}$$

Note that this reduces to $G^{\text{bare VMD}}$ when $|q^2|\to|p^2|$ and the parameter of Eq. (4.11b), $p\to 0$. To illustrate the relative behaviors of $G^{\mathrm{VMD}}_{q/\rho/\gamma}$ and $G^{\mathrm{PL}}_{q/\gamma}$ we examine the relative size of $W^{\mathrm{PL}}_{1\gamma}$ and $W^{\mathrm{VMD}}_{1\gamma}$ using the approximations (4.16) and (4.18) at $|q^2|=1.5$ $(\mathrm{GeV})^2$, for $\Lambda^2=(0.5\ \mathrm{GeV})^2$ and $|p^2|=m_\rho^2$, with $\bar{b}=8\frac{1}{3}(n_f=4)$. The $x\to 1$ approximations are plotted in Fig. 9(a). We see that, in the $x=0.6$ to 1 range where the $x\to$ approximation is not bad, the VMD contribution is at least a factor of 10 below the pointlike contribution. This discrepancy increases as $|q^2|$ increases—$W^{\mathrm{PL}}_{1\gamma}$ rises with $|q^2|$ while $W^{\mathrm{VMD}}_{1\gamma}$ falls with increasing $|q^2|$.

Of course, exact inversion is preferable.[21] We perform this for the pointlike contributions $G^{\mathrm{PL}}_{q_i/\gamma}$ of (3.15) and $W^{\mathrm{PL}}_{1\gamma}$ of (2.10). For the vector dominated contributions we first calculate the contribution from the quark portion of the bare VMD distribution by performing the convolution

$$G^{\mathrm{VMD}}_{q_i/\rho/\gamma}(q^2,m_\rho^2,x)=\sum_{\substack{q=u,\bar{u}\\ d,\bar{d}}}\int_x^1\frac{dz}{z}G^{\text{bare VMD}}_{q/\rho/\gamma}(z)\times G^{\mathrm{QCD}}_{q_i/q}\left(q^2,m_\rho^2,\frac{x}{z}\right) \tag{4.19}$$

where the moments of $G^{\mathrm{QCD}}_{q_i/q_j}$ are given in (3.16); we have set $|k^2|=m_\rho^2$ in $\xi(q^2,k^2)=\ln(|q^2|/\Lambda^2)/\ln(|k^2|/\Lambda^2)$. The usual k^2 integration in the convolution is absorbed implicitly into the $k_\perp$-integrated bare VMD distribution. We obtain for the per-color distribution moments

$$\int_0^1 x^{n-1}dx\,G^{\mathrm{VMD}}_{q/\rho/\gamma}(q^2,m_\rho^2,x)\underset{q=u,\bar{u},d,\bar{d}}{=}\gamma^q_{\rho,n}\left(h^n_D(\xi(q^2,m_\rho^2))+\frac{4}{2n_f}h^n_{\mathrm{ND}}(\xi(q^2,m_\rho^2))\right), \tag{4.20a}$$

$$\int_0^1 x^{n-1}dx\,G^{\mathrm{VMD}}_{q/\rho/\gamma}(q^2,m_\rho^2,x)\underset{q=s,\bar{s},c,\bar{c}}{=}\gamma^q_{\rho,n}\frac{4}{2n_f}h^n_{\mathrm{ND}}(\xi(q^2,m_\rho^2)), \tag{4.20b}$$

where the moment of the bare VMD distribution is

$$\gamma^q_{\rho,n}\equiv\int_0^1 dx\,x^{n-1}G^{\text{bare VMD}}_{q/\rho/\gamma}=\frac{C_\rho}{12}\frac{4\pi\alpha}{f_\rho^2}\frac{1}{n(n-1)} \tag{4.21}$$

In similar fashion, we find

$$\int_0^1 x^{n-1}dx\,G^{\mathrm{VMD}}_{g/\rho/\gamma}=4\gamma^q_{\rho,n}\frac{N}{N^2-1}h^n_G(\xi),$$

with h_G defined in (3.22). With these distributions it is then easy to calculate

$$\begin{aligned}2W^{\mathrm{PL}}_{1\gamma}&=e^2 3\sum_{i=1}^{2n_f}{Q_i}^2G^{\mathrm{PL}}_{q_i/\gamma},\\2W^{\mathrm{VMD}}_{1\gamma}&=e^2 3\sum_{i=1}^{2n_f}{Q_i}^2G^{\mathrm{VMD}}_{q_i/\rho/\gamma}.\end{aligned} \tag{4.22}$$

Of course, the above does not include the contributions to $W^{\mathrm{VMD}}_{1\gamma}$ of quarks which evolve from the gluon portion of the bare-VMD ρ wave-function content. We take (with $D_\rho=1.5$)

$$G^{\text{bare VMD}}_{g/\rho/\gamma}=\tfrac{1}{8}D_\rho\frac{(1-x)^2}{x}\frac{4\pi\alpha}{f_\rho^2}, \tag{4.23}$$

with moments

$$\int x^{n-1}dx\,G^{\text{bare VMD}}_{g/\rho/\gamma}\equiv\gamma^g_{\rho,n}=\frac{D_\rho}{8}\frac{2}{n(n^2-1)}\frac{4\pi\alpha}{f_\rho^2} \tag{4.23}$$

corresponding to dimensional counting $x\to 1$ behavior with 50% of the bare ρ's momentum in gluons. We then obtain a second contribution to the complete $G^{\mathrm{VMD}}_{q/\rho/\gamma}$. Thus

$$\int_0^1 x^{n-1}dx\,G^{\mathrm{VMD}}_{q_i/\rho/\gamma}(q^2,m_\rho^2,x)\underset{\text{any } q \text{ or } \bar{q}}{=}\gamma^g_{\rho,n}\bar{h}^n_{\mathrm{ND}}(\xi(q^2,m_\rho^2)) \tag{4.24}$$

where

$$\begin{aligned}\int_0^1 x^{n-1}dx\,G^{\mathrm{QCD}}_{q_i/g}&=\bar{h}^n_{\mathrm{ND}}(\xi(q^2,m_\rho^2))\\&=(\bar{D}^n_{12}\xi^{-\gamma_1}+\bar{D}^n_{11}\xi^{-\gamma_2}),\end{aligned} \tag{4.25}$$

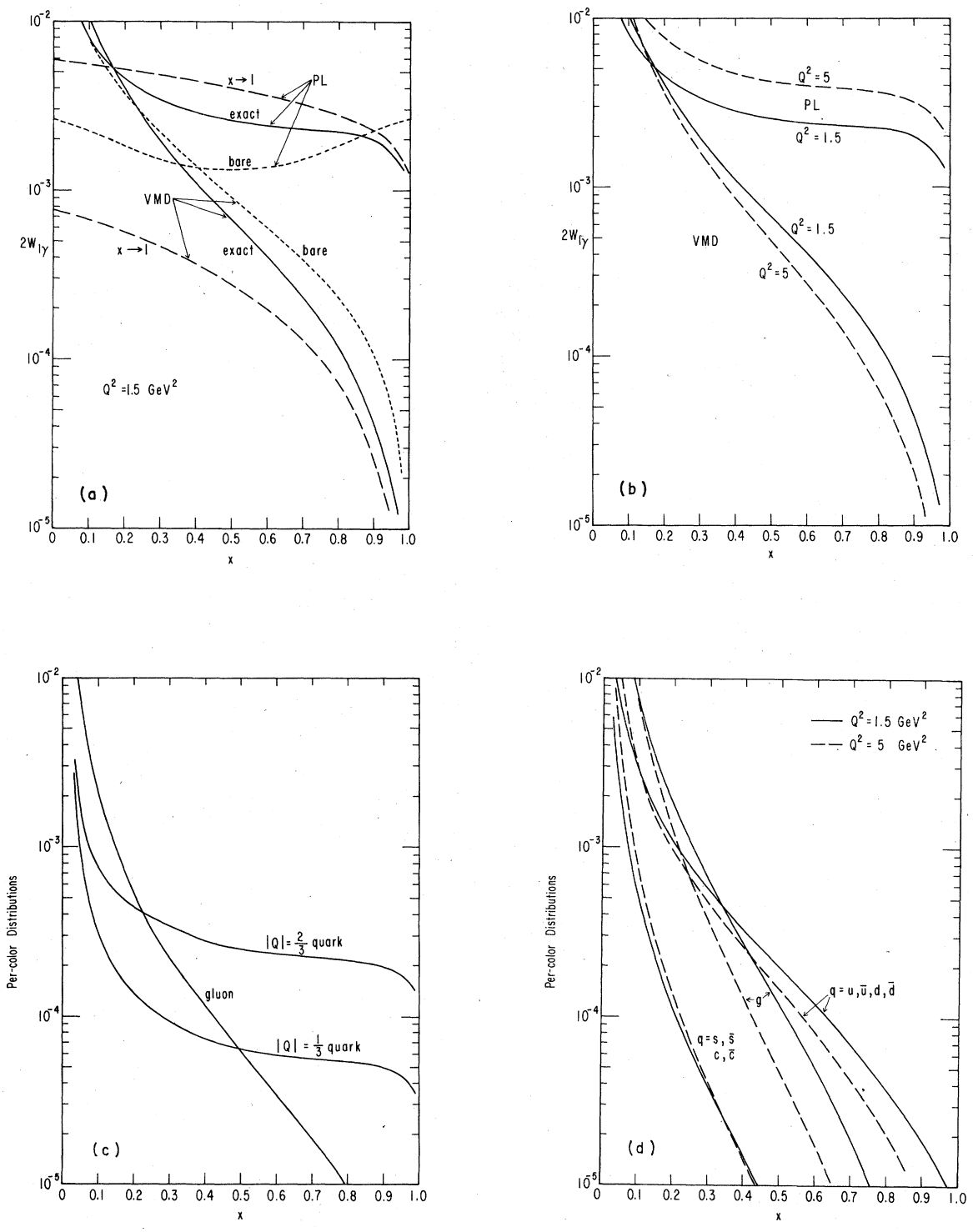

FIG. 9. (a) $2W_{1\gamma}$ as calculated in Sec. IV. The bare, QCD corrected, and QCD $x \to 1$ approximations are compared for both the VMD and the pointlike contributions at $Q^2 = 1.5$ GeV^2. (b) The full QCD corrected $2W_{1\gamma}$ contributions (PL and VMD) compared at $Q^2 = 1.5$ GeV^2. (c) The underlying quark and gluon distributions $G_{q/\gamma}$ and $G_{g/\gamma}$ of the photon target coming from the non-VMD, pointlike contributions. The common scaling factor $\ln Q^2/\Lambda^2$ is divided out. (d) The quark and gluon distribution functions $G_{q/\rho/\gamma}$ and $G_{g/\rho/\gamma}$ of the photon target coming from VMD contributions.

with

$$\bar{D}^n_{12}=-\bar{D}^n_{11}=\frac{C_2(R)}{8T(R)n_f}\frac{\gamma^n_{VF}}{b\delta^n}=\frac{N^2-1}{2Nn_f}\frac{\gamma^n_{VF}}{4b\delta^n}\,. \quad (4.26)$$

We can also easily calculate the corresponding contribution to $G^{\rm VMD}_{g/\rho/\gamma}$ using the moments of $G^{\rm QCD}_{g/g}$,

$$\int_0^1 x^{n-1}dx\,G^{\rm QCD}_{g/g}\equiv\bar{h}^n_G(\xi)=\bar{D}^n_{22}\xi^{-\gamma_1}+\bar{D}^n_{21}\xi^{-\gamma_2}\,, \quad (4.27)$$

with $\bar{D}^n_{22}=D^n_{12}$ and $\bar{D}^n_{21}=D^n_{11}$ [see Eq. (3.17)]. We obtain a contribution

$$\int_0^1 x^{n-1}dx\,G^{\rm VMD}_{g/\rho/\gamma}=\gamma^g_{\rho,n}\bar{h}_G(\xi) \quad (4.28)$$

per final gluon color.

The results for $2W_{1\gamma}$ are presented in Fig. 9(a) and compared to the bare-box and bare-VMD predictions and to the $x\to 1$ approximations. The $x\to 1$ approximations are seen to be good representations, on average, and correctly approach the exact predictions as $x\to 1$. The bare-box contribution is actually below the full result for $x<0.8$ (though of course, the $n=2$ momentum moments are the same) while the bare-VMD calculation is a substantial over estimate of the true result in the moderate to large x region; of course, as $Q^2\to m^2$ the full QCD-corrected VMD form approaches the bare-VMD form. The effect of the QCD corrections even for moderate Q^2 appear to make it easier to isolate experimentally the pointlike, totally calculable, contribution to $W_{1\gamma}$ over a substantial range of x.

In Fig. 9(b) we show the Q^2 dependence of the two different contributions to $2W_{1\gamma}$. As expected, the VMD contribution decreases, except at small x, as Q^2 increases, while the pointlike contributions continue to rise as $\ln(Q^2/\Lambda^2)$.

In Fig. 9(c) we give the pointlike contributions to the quark and gluon distribution functions (per color) as obtained by the exact inversion techniques.[21] We have divided out the overall factor, $\ln(Q^2/\Lambda^2)$.

In Fig. 9(d) we give the vector-dominance contributions to the quark and gluon distribution functions (per color) in a photon target, as obtained by the exact inversion, at $Q^2=1.5$ (GeV)^2 and 5 (GeV)^2.

Care must be exercised in using the pointlike contribution curves; the curves assume that u, d, s, *and* c quarks all contribute fully. Of course, in reality there are thresholds in $W^2=Q^2(1-x)/x$. At fixed $x=0.3$, for instance, $W^2\sim 3$ GeV^2 at $Q^2=1.5$ (GeV)^2 and the c contribution will be small; the correct result can be approximated by scaling according to the nonsinglet factor $\sum_{i=1}^{n_f}Q_i^4$,

$$\sum_{i=1}^{3}Q_i^4\Big/\sum_{i=1}^{4}Q_i^4=\frac{18}{34}\,.$$

At fixed Q^2 decreasing x will cause W^2 to increase and new thresholds will be systematically encountered.

The vector-dominance contributions are little affected by thresholds. In the nonsinglet approximation the initial ρ content $(u,d,\bar{u},\bar{d})$ is preserved and new thresholds are not seen. Only the small singlet corrections will be sensitive to quark thresholds.

B. Other short-distance phenomena

The distribution functions $G^{\rm PL}_{q_i/\gamma}$, the moments of which appear in (3.15), are probed in a large variety of situations.

1. High transverse momentum

(*a*) $\gamma\gamma$ *collisions*. This is studied exhaustively in Ref. 10. We first recall from the Introduction that the behavior $G^{\rm PL}_{q_i/\gamma}\propto\ln(Q^2/\Lambda^2)\tilde{f}(x)$ guarantees that the process of Fig. 5, based on quark-quark scattering, scales in leading-logarithmic order. The same arguments apply equally to the process of Fig. 10(a), which also produces four jets, two gluon jets at high p_T and two other at low p_T. The three-jet process of Fig. 10(b) is also exactly scaling. Here one incoming photon participates directly in the high-p_T subprocess, $\gamma q\to qg$; the subprocess cross section is proportional to $\alpha_s(4p_T^2)$ while the incoming quark distribution is proportional to $\alpha_s^{-1}(4p_T^2)$. The inclusive quark or gluon jet cross section thus scales exactly. A third process, which scales exactly is illustrated in Fig. 10(c). Here both incoming photons participate directly in the production of the two jets. There are no distribution functions involved and the $\gamma\gamma\to q\bar{q}$ subprocess cross-section scales exactly to leading-logarithmic accuracy. All QCD corrections are simply absorbed into the renormalized quark charges. It is easiest to visualize the calculation in terms of the imaginary part of an amplitude as illustrated in Fig. 11. Diagrams in which explicit gluon loops connect, for instance, the intermediate virtual quark and a final quark are suppressed by $\alpha_s(4p_T^2)$ in axial gauge (see Sec. III A of I); of course, there are implicit gluon corrections which are included in the wave func-

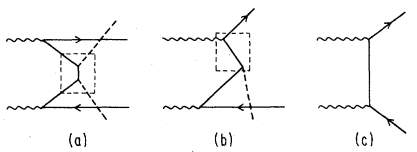

FIG. 10. Three additional (to that shown in Fig. 5) high-p_T jet production cross sections based on subprocesses (a) $qq\to gg$, (b) $\gamma q\to qg$, and (c) $\gamma\gamma\to q\bar{q}$.

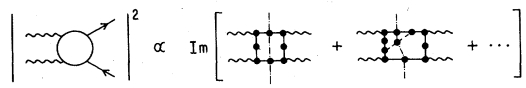

FIG. 11. The $\gamma\gamma \to q\bar{q}$ high-p_T cross section as an asymptotic series in fully renormalized diagrams, in the axial gauge.

tion (i.e., propagator) and vertex renormalizations represented by blobs in Fig. 11; these are eventually absorbed in the charge renormalization at the photon vertices—wave function and vertex renormalizations cancelling to give e_R. The first diagram of Fig. 11 would thus be computed as being proportional to

$$[e \ln(4p_T^2)^{-\bar{\gamma}_F}]^4[\ln(4p_T^2)^{\bar{\gamma}_F}]^4 = e^4 .$$

This is another illustration of the power of the axial gauge which makes this cancellation obvious. In Feynman gauge, for instance, both diagrams in Fig. 11 would contribute in $O(1)$ and only a full computation would reveal the appropriate cancellations.

Implicit in the above results is the assumption that the experimental calorimeter which observes the quark or gluon jet accepts the entire renormalized jet including QCD emission and reabsorption corrections, represented for instance by the renormalization blob in Fig. 11 (similar blobs are implicit in Fig. 10 and Fig. 5 but were not drawn). This is a nontrivial requirement as the renormalization of the propagator involves gluon-ladder loop integrations characterized by large momentum transfer Q^2 of order $4p_T^2$ itself (Fig. 12). The way to handle this requirement is illustrated by e^+e^- annihilation. That the total e^+e^- cross section computed as the imaginary part of the diagram illustrated in Fig. 13 should scale follows from the same type of argument as above—vertex corrections cancel propagator corrections. This scaling can be characterized as scaling of the cross section for production of jets. One looks at the entire event and then reconstructs the direction and total momentum of the jet. Similarly in $\gamma\gamma$ collisions one must look for a high p_T hadrons or an energetic calorimeter trigger as a signal for a high p_T jet, but then examine the entire event to decide the true direction and total p_T of the jet. In this way one can determine the cross section for production of a jet of given p_T and angular orientation.

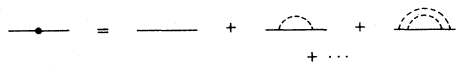

FIG. 12. The gluon structure implicit in a renormalized jet. The gluons nearest the short-distance subprocess have the largest p_T's relative to the final quark.

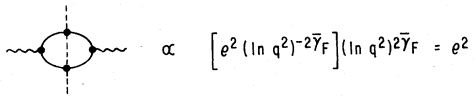

FIG. 13. e^+e^- annihilation total cross section as it would be calculated in leading-logarithm order in the axial gauge.

(*b*) *High-p_T γ production.*[22] If one looks at the cross section for production of a bare quark or hadron of given high p_T then scale breaking is introduced. Just as $G^{\rm QCD}_{q/q}(q^2,x)$ and

$$G_{q/T}(q^2,x) = \int_x^1 \frac{dz}{z}\, G^{\rm primordial}_{q/T}(z)\, G^{\rm QCD}_{q/q}(x/z, q^2)$$

exhibit scale violations so do the reverse decay functions.[22] In the realistic hadron case we are, as usual, faced with a lack of knowledge of the primordial (i.e., pre-QCD scale violation) decay distribution $D^{\rm primordial}_{H/q}(z)$. However, if we look at a final γ from the decay of a high-p_T jet the point like contributions dominate as they do in the reversed process of deep-inelastic scattering on a photon target. We obtain

$$D^{\rm PL}_{\gamma/q_i}(x,q^2) = \sum_{j=1}^{2n_f} \int d^2k_\perp \frac{dz}{z}\, D^{\rm Bare}_{\gamma/q_j}\left(\frac{x}{z}, k_\perp^2\right) \times G^{\rm QCD}_{q_j/q_i}(z, q^2, k^2) \qquad (4.29)$$

per color of q_i. Here $G^{\rm QCD}_{q_i/q_j}$ is color averaged for one quark and color summed in the other and

$$D^{\rm Bare}_{\gamma/q_j}(z,k^2) = \frac{e^2 Q_j^{\,2}}{8\pi^3}\, \frac{1+(1-z)^2}{z}\, \frac{1}{k_\perp^{\,2}} \qquad (4.30)$$

(also per q color) has moments

$$(D^{\rm Bare}_{\gamma/q_j})_n = \frac{e^2}{\pi}\, \frac{Q_j^{\,2}}{k_\perp^{\,2}}\, \hat{\gamma}_n \qquad (4.31a)$$

with

$$\hat{\gamma}_n = \frac{1}{8\pi^2}\, \frac{n^2+n+2}{n(n^2-1)} \qquad (4.31b)$$

analogous to (2.8). Retaining, for the moment, only the nonsinglet diagonal part of $G^{\rm QCD}_{q_j/q_i}$,

$$\int_0^1 z^{n-1}\, dz\, G^{\rm QCD}_{q_j/q_i}(q^2,k^2,z) = \delta_{ij}\left(\frac{\ln(|q^2|/\Lambda^2)}{\ln(|k|/\Lambda^2)}\right)^{-\gamma^n_{FF}/2b}, \qquad (4.32)$$

where δ_{ij} indicates diagonality in quark flavor (including q or $\bar{q}$ nature), we obtain

$$\int_0^1 x^{n-1}\, dx\, D^{\rm PL}_{\gamma/q_i}(x,q^2) = e^2 \ln\left(\frac{Q^2}{\Lambda^2}\right) Q_i^{\,2}\, \hat{f}_{{\rm NS},n} , \qquad (4.33)$$

where

$$\hat{f}_{\mathrm{NS},n} = \frac{\hat{\gamma}_n}{1+\gamma^n_{FF}/2b} \quad , \tag{4.34a}$$

and we define for later use

$$\hat{f}_{\mathrm{S},n} = \hat{\gamma}_n \ \frac{1+\gamma^n_{VV}/2b}{d_n} \ ; \tag{4.34b}$$

these are, of course, closely analogous to the definitions (2.10b). As in (3.15) we can generalize (4.33) to include the nonsinglet contributions with the result

$$\int_0^1 x^{n-1} dx \ D^{\mathrm{PL}}_{\gamma/q_i}(x,q^2)$$

$$= e^2 \ln\left(\frac{Q^2}{\Lambda^2}\right)\left(Q_i^{\,2}\hat{f}_{\mathrm{NS},n} + \frac{1}{n_f}\sum_{j=1}^{n_f} Q_j^{\,2}(\hat{f}_{\mathrm{S},n} - \hat{f}_{\mathrm{NS},n})\right) ; \tag{4.35}$$

clearly the only change has been the replacement of $\bar{\gamma}_n$ by $\hat{\gamma}_n$. This is intuitively correct since the distribution $D_{\gamma/q}$ is related to $G_{q/\gamma}$ by the reflection (both are per color of the quark)

$$D^{\mathrm{bare}}_{\gamma/q}(x) = x G^{\mathrm{bare}}_{q/\gamma}(1/x) \tag{4.36}$$

so that the moments are related by

$$\int_0^1 x^{n-1}\, dx\, D^{\mathrm{bare}}_{\gamma/q}(x) = \int_0^1 x^{n-1}\, dx\, x G^{\mathrm{bare}}_{q/\gamma}(1/x)$$

$$= \int_0^1 d\tau\, \tau^{-(n+1)-1} G^{\mathrm{bare}}_{q/\gamma}(\tau) \ , \tag{4.37}$$

i.e., by the $n \to -(n+1)$ reflection which converts $\bar{\gamma}_n$ into $\hat{\gamma}_n$. In (4.35) the $\hat{f}$'s contain γ^n_{FF}, γ^n_{VV} and (in d^n) γ^n_{FV}, γ^n_{VF}; these are defined through moments of $G^{\mathrm{Born}}_{q/q}$, $G^{\mathrm{Born}}_{g/g}$, and $G^{\mathrm{Born}}_{q/g}$, and $G^{\mathrm{Born}}_{g/q}$ (see Appendix A), respectively. The first two are symmetric under the reflection operation of (4.35) so that γ^n_{FF} and γ^n_{VV} are unchanged under reflection, while the product $\gamma^n_{FV}\,\gamma^n_{VF}$ is unchanged under reflection. Thus (4.35) guarantees that the reciprocity relation

$$D^{\mathrm{PL}}_{\gamma/q}(x,q^2) = x G^{\mathrm{PL}}_{q/\gamma}(1/x,q^2) \tag{4.38}$$

holds after including all leading-logarithmic corrections.

An analogous result for gluon decay into a γ is also easily obtained, by reflection arguments, from the result (3.15). We would compute the per color decay into a γ as

$$D^{\mathrm{PL}}_{\gamma/g}(x,q^2) = \frac{N}{N^2-1}\sum_{i=1}^{2n_f}\int d^2k_\perp \frac{dz}{z} D^{\mathrm{bare}}_{\gamma/q_i}\left(\frac{x}{z},k^2\right) \times G^{\mathrm{QCD}}_{q_i/g}(z,q^2,k^2) \ , \tag{4.39}$$

where $G^{\mathrm{QCD}}_{q_i/g}$ is summed over gluon colors and averaged over q_i colors, in our standard definition. Note that we have reversed the gluon-quark transition. The result for $G^{\mathrm{QCD}}_{q_i/g}$ is obtained from $[(N^2-1)/N]\ G^{\mathrm{QCD}}_{g/q_i}$ [see Eq. (3.22)] by changing n to $-(n+1)$ in the moments; the factor $(N^2-1)/N$ converts the gluon-color average to a color sum and the quark-color sum to a quark-color average. The net result, analogous to (3.25), is then

$$D^{\mathrm{PL}}_{\gamma/g}(x,q^2)x^{n-1}dx = \frac{4N}{N^2-1}\ln\left(\frac{Q^2}{\Lambda^2}\right)e^2 \times \sum_{i=1}^{n_f} Q_i^{\,2}\frac{\hat{\gamma}_n}{2bd_n}\left(\frac{\gamma^n_{VF}C_2(R)}{8T(R)n_f}\right)$$

$$= \tfrac{1}{2}\ln\left(\frac{Q^2}{\Lambda^2}\right)e^2\sum_{i=1}^{n_f} Q_i^{\,2}\hat{\gamma}_n\frac{\gamma^n_{VF}/n_f}{2b\,d_n} \ , \tag{4.40}$$

where we have used

$$\gamma^{-(n+1)}_{FV} = \frac{C_2(R)}{8T(R)n_f}\ \gamma^n_{VF} \ ,$$

$$\gamma^{-(n+1)}_{FV}\gamma^{-(n+1)}_{VF} = \gamma^n_{FV}\gamma^n_{VF} \ , \tag{4.41}$$

and

$$\frac{NC_2(R)}{N^2-1} = T(R) \ . \tag{4.42}$$

The result (4.40) is more trivially obtained directly from (3.25) by $n \to -(n+1)$ reflection and use of (4.41) and (4.42).

These distributions may be used to make precise predictions for high-p_T γ production in collisions of various types as well as for γ production in the jets of e^+e^- annihilation. The two most important features of the γ distribution are its enhancement with $\ln Q^2$ and its very weak suppression as $z \to 1$

$$D^{\mathrm{PL}}_{\gamma/q}(z,q^2) \underset{z\to 1}{\sim} \alpha\frac{\ln(Q^2/\Lambda^2)}{\ln[\,1/(1-z)]} \tag{4.43}$$

[see (4.16)]. As the edge of phase space is approached ($2p^\gamma_T/\sqrt{s} \to 1$ in high-p_T collisions, $2|\,p^\gamma|\,/\sqrt{s} \to 1$ in e^+e^- annihilation) single-γ production will actually become comparable to single-hadron production for which the decay distributions are suppressed by a power in $(1-z)$

and by an overall q^2 dependent suppression factor; for instance [see Eq. (4.18)]

$$D_{\pi/q}(z,q^2) \underset{z\to 1}{\sim} (1-z)^{1+p(q^2)} \frac{e^{(3/4-\gamma_E)p(q^2)}}{\Gamma(p(q^2)+2)} . \tag{4.44}$$

The effects of this weaker suppression have already been surveyed in papers by Rückl, Gunion, and Brodsky and by Jones and Rückl (see Ref. 22). One finds that at high p_T the γ/π ratio coming from jet fragmentation can approach 1 for

$$\frac{2p_T^{\gamma \text{ or } \pi}}{\sqrt{s}} > 0.8 .$$

However, the high-p_T cross section is dominated by diagrams in which the γ participates directly in the high-p_T subprocess and thus $D_{\gamma/q}$ is not probed. This is restated diagrammatically in Fig. 14. Tests of this weaker fragmentation suppression will thus be easiest in e^+e^- annihilation. In high-p_T physics one must distinguish between diagram (a) and (b) of Fig. 14 by noting that if the γ participates directly in the high-p_T subprocess (a) then it is produced on its own, i.e., without accompanying hadrons; whereas if it is the fragment of a quark jet, (b), it has an accompanying jet of hadrons. Diagrams of type (b) generally are only a small percentage of the total high-p_T γ cross section.

2. $\mu^+\mu^-$ pair production, etc.

In this category we include any reaction in which a quark (or antiquark) from an incoming photon target is used to make a massive object $\Gamma, \psi, \mu^+\mu^-$ pair, etc., —via the usual $q\bar{q}$ annihilation method, Fig. 15. In the leading-logarithmic order the ladder structure of the theory (in axial gauge) guarantees that it is correct to use the $G_{q/\gamma}(q^2,x)$ as measured in deep-inelastic scattering on a photon target to calculate the massive particle (or pair) production cross section. This is true in γN and $\gamma\gamma$ collisions. The shape of the $G_{q/\gamma} = G_{\bar{q}/\gamma}$ distribution function illustrated in Fig. 9(c) shows that the relative probability of finding fast quarks or antiquarks in a photon source is much higher than for a hadron source [see Fig. 9(d)] where fast fragments are suppressed by a power [see (4.16) vs. (4.18) for example]. Thus the large-mass portion of the μ-pair spectrum in γN collisions will be greatly enhanced relative to the μ-pair spectrum observed in a purely hadronic collisions such as πN. Correspondingly the massive particle or μ pair will have a broader distribution (at any given mass) in x_F—its longitudinal-phase-space location—in γ initiated collisions.

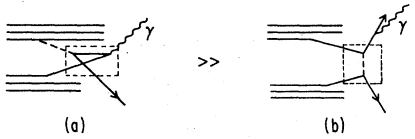

FIG. 14. Mechanisms for production of a high-p_T γ in pp collisions. (a) dominates over (b) but is distinguishable by the absence of an accompanying quark jet of hadrons.

V. CONCLUSION

Thus we have seen that the photon again reveals itself to be a particularly simple object. When the photon's distribution functions $G_{q_i/\gamma}$, D_{γ/q_i}, $G_{g/\gamma}$, and $D_{\gamma/g}$ are probed at large momentum transfer q^2 by any short-distance process, all the above exhibit extremely simple and exactly calculable scaling behavior, for instance

$$G_{q_i/\gamma}(x,q^2) \propto \ln(Q^2/\Lambda^2) f_{q_i/\gamma}(x) . \tag{5.1}$$

The moments of the pointlike contributions to the G's and D's appear in equations (3.15), (3.25), (4.35), and (4.40). Thus reactions involving two photon collisions take on special significance as they are exactly calculable to leading-logarithmic accuracy in QCD. For instance many of the high-p_T jet production cross sections are then predicted to exhibit exact scaling. We have also estimated the full QCD-corrected vector-dominance background to the above G distributions. These appear in Eqs. (4.20), (4.23), (4.24), and (4.28). For moderate Q^2 (> 1.5 GeV^2) they are relatively small over much of the x range.

In addition, we have rederived the earlier results for deep-inelastic scattering on a photon target obtained by Witten.[8] The leading contributions to $W_{1\gamma}$ and $W_{L\gamma}$, Eqs. (2.10) and (2.18) are exactly calculable and according to estimates are likely to far exceed vector-dominance backgrounds over a substantial range of $x = 1/\omega$.

Finally in Appendix B we present a convenient summary of QCD corrections through the full leading-logarithmic forms of $G_{q/q}^{\text{QCD}}$, $G_{q/g}^{\text{QCD}}$, $G_{g/g}^{\text{QCD}}$, and $G_{g/g}^{\text{QCD}}$.

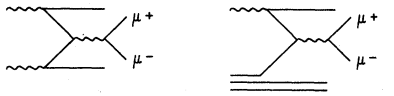

FIG. 15. Massive-pair production in $\gamma\gamma$ and γN collisions.

ACKNOWLEDGMENTS

We wish to acknowledge helpful conversations with S. Brodsky, T. De Grand, and D. Jones. The first two are involved with work quite similar to our own. During the course of preparation of this manuscript closely related works by C. H. Llewellyn Smith[23] and by DeWitt *et al.*[24] have appeared. One of us (J.F.G.) would like to acknowledge the generous support of the A. P. Sloan Foundation. We would like to acknowledge the support of the Aspen Institute for Physics where this work was begun and one of us (J. F.G.) wishes to thank the Seattle Summer Institute for its support during the writing of the manuscript. This work was supported in part by the U. S. Department of Energy.

APPENDIX A: PARAMETERS USED IN CALCULATIONS

In this appendix we accumulate some of the important parameters which go into the photon-structure-function calculations. These were all derived in I. First the anomalous dimensions ($16\pi^2 b = \bar{b}$)

$$\frac{\gamma_{FF}^n}{2b} = \frac{1}{\bar{b}}\left(1 - \frac{2}{n(n+1)} + 4\sum_{j=2}^{n}\frac{1}{j}\right)\left(\frac{4}{3}\right), \tag{A1a}$$

$$\frac{\gamma_{VV}^n}{2b} = \frac{1}{\bar{b}}\left(\frac{1}{3} - \frac{4}{n(n-1)} - \frac{4}{(n+1)(n+2)} + 4\sum_{j=2}^{n}\frac{1}{j}\right) \tag{A1b}$$

$$+ \frac{1}{\bar{b}}\,\frac{4}{3}\,n_f\left(\frac{1}{2}\right),$$

$$\frac{\gamma_{VF}^n}{2b} = \frac{1}{\bar{b}}\,\frac{n^2+n+2}{n(n^2-1)}\left(\frac{4}{3}\right), \tag{A1c}$$

$$\frac{\gamma_{VF}^n}{2b} = \frac{8}{\bar{b}}\,\frac{n^2+n+2}{n(n+1)(n+2)}\,n_f\left(\frac{1}{2}\right). \tag{A1d}$$

The constants in parentheses refer to the group-theoretical constants $C_2(G)=3$, $C_2(R)=\frac{4}{3}$, $T(R)=\frac{1}{2}$ (per fermion flavor); n_f is the number of q flavors. In I, for example, $\gamma_{FF}/2b$ was computed as

$$\frac{\gamma_{FF}^n}{2b} = \bar{\gamma}_F - \frac{b_{FF}^n}{b}, \tag{A2}$$

where

$$\frac{b_{FF}^n}{b} = \frac{1}{8\pi^2 b}\int dz\, z^{n-1}\,\frac{1+z^2}{1-z}\,C_2(R) \tag{A3}$$

is a moment of the lowest-order QCD distribution for a quark-from-a-quark of the same type; for large $k_\perp{}^2$

$$G_{q/q}(z, k_\perp{}^2) \sim \frac{4}{3}\,\frac{\alpha_s(k_\perp{}^2)}{2\pi}\,\frac{1+z^2}{1-z}\,\frac{1}{k_\perp{}^2}\,C_2(R). \tag{A4}$$

[Here $z = (p_0' + p_3')/(p_0 + p_3)$ and $k_\perp = p_\perp'$ in a frame with $p_\perp = 0$, p' and p are the momenta of the secondary and primary quark, respectively.] The other ingredient, $\bar{\gamma}_F$, the propagator anomalous dimension, is the $n=1$ "probability" moment

$$\bar{\gamma}_F = \frac{b_{FF}^1}{b}, \tag{A5}$$

Next we repeat the expression for the moments of the "Born" terms of the Bethe-Salpeter equations for T_1 and T_L in I. We obtained

$$F_{1,n}^i = 2Q_i{}^2, \quad G_{1,n}^i = 0$$

$$F_{L,n}^i = \frac{Q_i{}^2 C_2(R)}{2\pi^2 b \ln|q^2|}\,\frac{1}{n+1}, \tag{A6}$$

$$G_{L,n} = \frac{2\sum_{i=1}^{n_f} Q_i{}^2 T(R)}{\pi^2 b \ln|q^2|}\,\frac{1}{(n+1)(n+2)},$$

when both uncrossed and crossed virtual-photon graphs were included. We also use several times the identity from Appendix IC

$$\frac{C_{11}^{\alpha,n}}{1+\gamma_1^n} + \frac{C_{12}^{\alpha,n}}{1+\gamma_2^n} = \frac{1}{d_n}\left[F_{\alpha,n}(1+\gamma_{VV}^n/2b) + G_{\alpha,n}\gamma_{FV}^n/2b\right]. \tag{A7}$$

APPENDIX B: COMPENDIUM OF DISTRIBUTION FUNCTIONS[25]

We summarize in our language the crucial results for the QCD evolution functions $G_{q_i/q_j}^{\rm QCD}$, $G_{q_i/g}^{\rm QCD}$, $G_{g/q_i}^{\rm QCD}$, and $G_{g/g}^{\rm QCD}$. Their moments are a function of $\xi = \ln(|q^2|/\Lambda^2)/\ln(|k^2|/\Lambda^2)$, where q^2 is the off-shell mass of the final q or g. This off-shell mass becomes essentially the same as the mass of the short-distance probe in leading-logarithmic order [see I(2.5)]. The variable k^2 is the mass of the initial q_j. G_{g/q_i} and $G_{q_i/g} \to 0$ as $|q^2| \to |k^2|$, while G_{q_i/q_j} and $G_{g/g} \to$ appropriate δ functions in this limit. Each G is averaged over colors of the final particle and summed over colors of the initial. They are to be folded together with per color primordial target, T, distribution functions $G_{b/T}^{\rm primordial}$ (assumed to have strong k_T damping)

$$G_{a/T}^{\text{QCD-corrected}}(x, |q^2|, m_T{}^2) = \sum_{\substack{b=q,\bar{q}\\ g}} \int_x^1 \frac{dz}{z}\, G_{b/T}^{\text{primordial}}(z) G_{a/b}^{\rm QCD}\left(\frac{x}{z}, |q^2|, m_T{}^2\right) \tag{B1}$$

to obtain the per-color QCD-corrected target distribution functions, $G_{a/T}^{\text{QCD-corrected}}$ (we have taken

$\langle |k^2| \rangle \sim m_T^2$ for simplicity). The $\sum_b$ does not include colors; the color sum for $\sum_b$ is incorporated in our definition of $G_{a/b}^{\mathrm{QCD}}$. We have obtained the moments

$$(G_{q_i/q_j})_n = \delta_{ij}\xi^{-\gamma_{11}^n} + \frac{1}{2n_f}(\xi^{-\gamma_1^n}D_{11}^n + \xi^{-\gamma_2^n}D_{12}^n - \xi^{-\gamma_{11}^n}), \tag{B2a}$$

$$(G_{g/q_i})_n = \frac{N}{N^2-1}(\xi^{-\gamma_1^n} - \xi^{-\gamma_2^n})\frac{2\gamma_{12}^n}{\delta^n}, \tag{B2b}$$

$$(G_{q_i/g})_n = \frac{N^2-1}{2Nn_f}(\xi^{-\gamma_1^n} - \xi^{-\gamma_2^n})\frac{\gamma_{21}^n}{2\delta^n}, \tag{B2c}$$

$$(G_{g/g})_n = (\xi^{-\gamma_1^n}D_{12}^n + \xi^{-\gamma_2^n}D_{11}^n). \tag{B2d}$$

Here

$$\xi = \ln(|q^2|/\Lambda^2)/\ln(|k^2|/\Lambda^2) \tag{B3}$$

and

$$\gamma_{1,2}^n = \tfrac{1}{2}(\gamma_{11}^n + \gamma_{22}^n \mp \delta^n),$$
$$\delta^n = [\gamma_{11}^n - \gamma_{22}^n)^2 + 4\gamma_{12}^n\gamma_{21}^n]^{1/2},$$
$$D_{11}^n = \frac{\delta^n - \gamma_{11}^n + \gamma_{22}^n}{2\delta^n}, \quad D_{12}^n = \frac{\delta^n + \gamma_{11}^n - \gamma_{22}^n}{2\delta^n} \tag{B4}$$

we have used the notation

$$\gamma_{11}^n = \frac{\gamma_{FF}^n}{2b}, \quad \gamma_{22}^n = \frac{\gamma_{VV}^n}{2b}, \quad \gamma_{12}^n = \frac{\gamma_{FV}^n}{2b}, \quad \gamma_{21}^n = \frac{\gamma_{VF}^n}{2b}$$

with the γ_{FF}, etc., of Appendix A. It can, of course, be verified that the $n=2$ moment is conserved under evolution. Using $\delta^{n=2} = \gamma_{11}^{n=2} + \gamma_{22}^{n=2}$, $\gamma_{21}^{n=2} = 2\gamma_{22}^{n=2}$, and $2\gamma_{12}^{n=2} = \gamma_{11}^{n=2}$ we find

$$\frac{1}{(N^2-1)}(2n_fNG_{q_i/g} + (N^2-1)G_{g/g})_{n=2} = 1, \tag{B5a}$$

$$\frac{1}{N}\left(N\sum_{i=1}^{2n_f} G_{q_i/q_j} + (N^2-1)G_{g/q_j}\right)_{n=2} = 1, \tag{B5b}$$

verifying explicitly gluon-momentum and quark-momentum conservation, respectively.

We also note that the derivatives $(-dG/d\xi)_{\xi\to 0}$ give the lowest-order contributions to the G's in the ladder development discussed in paper I:

$$-\frac{d}{d\xi}(G_{q_i/q_j})_n\big|_{\xi=0} = \delta_{ij}\gamma_{11}^n, \tag{B6a}$$

$$-\frac{d}{d\xi}(G_{g/q_i})_n\big|_{\xi=0} = 2\gamma_{12}^n\frac{N}{N^2-1}, \tag{B6b}$$

$$-\frac{d}{d\xi}(G_{q_i/g})_n\big|_{\xi=0} = \frac{N^2-1}{2Nn_f}\frac{\gamma_{21}^n}{2}, \tag{B6c}$$

$$-\frac{d}{d\xi}(G_{g/g})_n\big|_{\xi=0} = \gamma_{22}^n. \tag{B6d}$$

Each is the correctly normalized moment of the lowest transitions: (a) $q \to q + (g)$; (b) $q \to g + (q)$; (c) $g \to q + (\bar{q})$; and (d) $g \to [g + (g)] + [g + (q)]$, respectively. The particles in parentheses are the spectators to the probed particle.

Following the procedures discussed in Sec. IV we may obtain forms for the distributions valid as $x \to 1$. We use the large-n limits (see Appendix A)

$$\gamma_{11}^n \sim \frac{4}{b}C_2(R)(\ln n + \gamma_E - \tfrac{3}{4}), \tag{B7a}$$

$$\gamma_{22}^n \sim \frac{4}{b}C_2(G)\left(\ln n + \gamma_E - \frac{11}{12} + \frac{n_fT(R)}{3C_2(G)}\right), \tag{B7b}$$

$$\gamma_{12}^n \sim \frac{1}{b}\frac{1}{n}C_2(R), \tag{B7c}$$

$$\gamma_{21}^n \sim \frac{8}{b}\frac{1}{n}n_fT(R) \tag{B7d}$$

and

$$D_{11}^n \to 1, \quad \gamma_1^n \to \gamma_{11}^n$$
$$\delta^n \to \gamma_{22}^n - \gamma_{11}^n, \tag{B8}$$
$$D_{12}^n \to 0, \quad \gamma_2^n \to \gamma_{22}^n$$

which yield (note that $\gamma_{2n}^n \gtrsim_\infty \gamma_1^n$ for $C_2(G) > C_2(R)$ so $\xi^{-\gamma_1^n} \overset{n\to\infty}{\gg} \xi^{-\gamma_2^n}$)

$$(G_{q_i/q_j})_n \sim \delta_{ij}\xi^{-\gamma_{11}^n}, \tag{B9a}$$

$$(G_{g/q_i})_n \sim \frac{N}{N^2-1}\xi^{-\gamma_{11}^n}\frac{C_2(R)}{2n\Delta_n}, \tag{B9b}$$

$$(G_{q_i/g})_n \sim \frac{N^2-1}{2Nn_f}\xi^{-\gamma_{11}^n}\frac{n_fT(R)}{n\Delta_n}, \tag{B9c}$$

$$(G_{g/g})_n \sim \xi^{-\gamma_{22}^n}, \tag{B9d}$$

$$\Delta_n = [C_2(G) - C_2(R)](\ln n + \gamma_E) + \tfrac{3}{4}C_2(R) - \tfrac{11}{12}C_2(G) + \frac{n_fT(R)}{3}.$$

The form (B9a) was inverted in Sec. IV and the form (B9d) is entirely analogous. The result is essentially obtained by the intuitive substitution $n \sim (1/1-x)$ (i.e., the larger the moment, the nearer 1 the x value probed) accompanied by appropriate normalization. We obtain

$$G_{q_i/q_j}(x,\xi) \underset{x\to 1}{\sim} \delta_{ij}(1-x)^{\bar{p}-1} \times \frac{\exp\{[4C_2(R)/\bar{b}]\ln\xi(3/4-\gamma_E)\}}{\Gamma(4C_2(R)\ln\xi/\bar{b})}, \tag{B10a}$$

where $\bar{p} = [4C_2(R)/\bar{b}]\ln\xi$

$$G_{g/g}(x,\xi) \underset{x\to 1}{\sim} (1-x)^{\bar{p}-1} \frac{\exp\{[4C_2(G)/\bar{b}]\ln\xi[11/12 - \gamma_E - n_fT(R)/3C_2(G)]\}}{\Gamma(4C_2(G)\ln\xi/\bar{b})}, \tag{B10b}$$

where $\bar{p} = [4C_2(G)/\bar{b}]\ln\xi$

The off-diagonal distributions (B9b) and (B9c) are inverted in entirely similar fashion. The $1/n$ in the moments indicates a basic power $(1-x)^p$ rather than $(1-x)^{p-1}$, as for the diagonal elements, where $p=[4C_2(R)/\bar{b}]\ln\xi$ as appropriate to $\xi^{-\gamma_1^n}$; the $1/\ln n$ is correctly incorporated by the substitution $n\to 1/1-x$ as was the case for $G_{g/\gamma}$ in Sec. IV. The normalization is determined as in the case of (B9a) discussed in Sec. IV. We obtain

$$G_{g/q_i}(x,\xi)\underset{x\to 1}{\sim}\frac{N}{N^2-1}(1-x)^p\left(\frac{C_2(R)}{2\Delta(x)}\right),$$
$$\Delta(x)=[C_2(G)-C_2(R)]\left(\ln\frac{1}{1-x}+\gamma_E\right)+\tfrac{3}{4}C_2(R)-\tfrac{11}{12}C_2(G)+\frac{n_f T(R)}{3} \tag{B10c}$$

and

$$G_{q_i/g}(x,\xi)\underset{x\to 1}{\sim}\left(\frac{N^2-1}{N}\right)G_{g/q_i}(x,\xi). \tag{B10d}$$

The latter result is intuitively obvious since $G_{q_i/g}$ and G_{g/q_i} should be related by $x\to 1/x$ as $x\to 1$ aside from different color average and sum factors. The general features of these $x\to 1$ results are intuitively sensible. A gluon $\to$ gluon transition is controlled by the Casimir operator $C_2(G)$ while the quark $\to$ quark transition is controlled by $C_2(R)$ where $C_2(G)/C_2(R)=\frac{9}{4}$, a ratio which is encountered in gluon vs quark jet multiplicity ratios. Note that for large enough ξ a gluon prefers to use the "off-diagonal" decay into a quark rather than decay into a gluon. This occurs (roughly) when

$$\frac{4C_2(G)\ln\xi}{\bar{b}}-1>\frac{4C_2(R)\ln\xi}{\bar{b}}. \tag{B11}$$

Finally we note the result, proved in Sec. IV for a few special cases, that decay distributions, D, including all leading-logarithmic corrections are simply obtained by the reciprocity relation

$$D_{a/b}(x,q^2)=xG_{b/a}\left(\frac{1}{x},q^2\right) \tag{B12}$$

at the quark and gluon level. This remains valid even after the quark and gluon decay distributions are folded together with primordial hadron or photon source distributions. The preceding formulas thus allow an economical summary of all leading-order QCD corrections.

---

[1]S. J. Brodsky, T. Kinoshita, and H. Terazawa, Phys. Lett. 27, 280 (1971).

[2]D. Gross and S. Treiman, Phys. Rev. D 4, 2105 (1971).

[3]There is some disagreement in normalization conventions in the literature. We define W_1 and W_2 in the conventional manner $W_1=(1/2\pi)\,\mathrm{Im}\,T_1$, $W_2=(1/2\pi)\,\mathrm{Im}\,T_2$ where the target-spin-averaged amplitude for $\gamma_\mu^*(q)$ target $\to\gamma_\nu^*(q)$ target has the decomposition

$$T_{\mu\nu}=T_1\left(-g_{\mu\nu}+\frac{q_\mu q_\nu}{q^2}\right)+T_2\left(p_\mu-q_\mu\frac{p\cdot q}{q^2}\right)\left(p_\nu-q_\nu\frac{p\cdot p}{q^2}\right).$$

In this normalization (for $W_L/W_1\to 0$)

$$2W_1\sim\frac{\nu W_2}{x}=e^2\sum_{\substack{\text{all } q,\bar{q}\\ \text{color}}}Q_i^{\,2}G_{q_i/\text{target}},$$

where $G_{q_i/\text{target}}$ is the probability distribution for quarks of type i in the target. Note that quarks and antiquarks must be separately summed over, yielding a factor of 2 which we often write explicitly later in the paper.

[4]It is interesting to note that $(W_{1\gamma})_{\text{Box}}$ and $(W_{L\gamma})_{\text{Box}}$ both receive their leading contributions from only the uncrossed box diagram of Fig. 3 if an axial gauge for the real γ is employed. If a Feynman-gauge replacement $\sum\epsilon_\alpha\epsilon_\beta^*=-g_{\alpha\beta}$ is made for the $\gamma(p)$ polarization sum the situation changes; $(W_{L\gamma})_{\text{Box}}$, for instance, gets a contribution in leading order only from the crossed diagrams.

[5]T. Walsh and P. Zerwas, Nucl. Phys. B41, 551 (1972).

[6]R. L. Kingsley, Nucl. Phys. B60, 45 (1973).

[7]R. P. Worden, Phys. Lett. 51B, 57 (1974). M. A. Ahmed and G. G. Ross, Phys. Lett. 59B, 369 (1975).

[8]E. Witten, Nucl. Phys. B120, 189 (1977).

[9]W. R. Frazer and J. F. Gunion, Phys. Rev. D 19, 2447 (1979).

[10]S. J. Brodsky, T. De Grand, J. F. Gunion, and J. Weis, Phys. Rev. D 19, 1418 (1979); Phys. Rev. Lett. 41, 672 (1978).

[11]Our notation is $\gamma_{FF}^n/2b=\bar{\gamma}_F-b_{FF}^n/b$, etc., $\bar{\gamma}_F$ and b_{FF}^n are given in I. $\gamma_{FF}^n/2b$ is essentially the anomalous dimension of the quark nonsinglet structure function, which behaves as $(\ln q^2)^{-\gamma_{FF}^n/2b}$. Changing our notation from I, we have incorporated the n_f factor in γ_{VF}; see Appendix A.

[12]L. N. Lipatov, Yad. Fiz. 20, 181 (1974) [Sov. J. Nucl. Phys. 20, 94 (1975)]; 20, 532 (1974) [20, 287 (1975)].

[13]Recall that since T_1 includes both orderings of the virtual $\gamma^*(q)$'s, only one of which has an imaginary part, an expansion $T_1=\sum a_n\omega^n$ yields moments of $W_1=(1/2\pi)\mathrm{Im}T_1$ through $\int W_1 x^{n-1}dx=\frac{1}{4}a_n$.

[14]W. A. Bardeen and A. J. Buras, Phys. Rev. D 20, 166 (1979). The $\ln[\ln(Q^2/\Lambda^2)]/\ln(Q^2/\Lambda^2)$ correction is given in J. F. Gunion and D. Jones, Report No. UCD-79-2 (unpublished).

[15]See Ref. 10 for more information on this bare vector-dominance distribution.

[16]The derivation which follows is similar to that which

appears in Ref. 10.

[17]These results were also obtained by Y. Dokshitser, D. D'Yakanov, and S. Troyan, Proceedings of the 13th Winter School of the Leningrad B. P. Konstantinov Institute of Nuclear Physics, 1978, SLAC Report No. SLAC-TRANS-183 (unpublished).

[18]A thorough exposition of $x \to 1$ behaviors has also been developed by T. De Grand, Report No. UCSB-TH-15, 1978 (unpublished) which was received as this paper was being typed.

[19]We ignore quarks which arise from gluons in the ρ. As $x \to 1$ $G_{\ell/\rho/\gamma}^{\text{bare, VMD}} \sim (1-x)^2$ from dimensional counting which yields a higher power of $(1-x)$ than in (4.18).

[20]Again similar manipulations appear in Ref. 18.

[21]We use the method of F. J. Yndurain, Phys. Lett. 74B, 68 (1978).

[22]This has been studied by many authors. We list only a few: R. Rückl, S. J. Brodsky, and J. F. Gunion, Phys. Rev. D 18, 2469 (1978); D. Jones and R. Rückl, UCD Report No. 78-4 (unpublished); G. R. Farrar and S. Frautschi, Phys. Rev. Lett. 36, 1017 (1976); F. Halzen and D. M. Scott, *ibid.* 40, 1117 (1978); C. H. Llewellyn Smith, Phys. Lett. 79B, 83 (1978); K. Koller, T. F. Walsh, and P. M. Zerwas, DESY Report No. DESY 78/77 (unpublished).

[23]C. H. Llewellyn Smith, Phys. Lett. 79B, 83 (1978).

[24]R. J. DeWitt, L. M. Jones, J. D. Sullivan, D. E. Willen, and H. W. Wyld, Phys. Rev. D 19, 2046 (1979).

[25]The results of this section are an improved summary of those of paper I. Similar information is contained in the following papers: G. Altarelli and G. Parisi, Nucl. Phys. B126, 298 (1977); Ref. 17; Ref. 18. The results are entirely equivalent to those obtained by the usual renormalization-group approach. See H. D. Politzer, Phys. Rep. 14C, 129 (1974) for a review. The basic intuition follows the parton approach of J. Kogut and L. Susskind, Phys. Rev. D 9, 697 (1974). The basic ingredients in these results also appear in D. Amati, R. Petronzio, and G. Veneziano, Nucl. Phys. B140, 54 (1978); Report No. CERN TH 2527, 1978 (unpublished); Y. Kazama and Y.-P. Yao, Phys. Rev. Lett. 41, 611 (1978); C. H. Llewellyn Smith, lectures presented at the XVIIth Internationale Universitatswochen für Kerphysik, Schladming, 1978 (unpublished); and K. J. Kim and K. Schilcher, Phys. Rev. D 17, 2800 (1978).